**NASA TECHNICAL**
**MEMORANDUM**

NASA TM X-3379

# NOISE REDUCTION TESTS OF LARGE-SCALE-MODEL EXTERNALLY BLOWN FLAP USING TRAILING-EDGE BLOWING AND PARTIAL FLAP SLOT COVERING

*Daniel J. McKinzie, Jr., Robert J. Burns,*
*and Jack M. Wagner*

*Lewis Research Center*
*Cleveland, Ohio 44135*

| 1. Report No.<br>NASA TM X-3379 | 2. Government Accession No. | 3. Recipient's Catalog No. |
|---|---|---|
| 4. Title and Subtitle NOISE REDUCTION TESTS OF LARGE-SCALE-MODEL EXTERNALLY BLOWN FLAP USING TRAILING-EDGE BLOWING AND PARTIAL FLAP SLOT COVERING | | 5. Report Date<br>April 1976 |
| | | 6. Performing Organization Code |
| 7. Author(s)<br>Daniel J. McKinzie, Jr., Robert J. Burns, and Jack M. Wagner | | 8. Performing Organization Report No.<br>E-8598 |
| 9. Performing Organization Name and Address<br>Lewis Research Center<br>National Aeronautics and Space Administration<br>Cleveland, Ohio 44135 | | 10. Work Unit No.<br>505-03 |
| | | 11. Contract or Grant No. |
| | | 13. Type of Report and Period Covered<br>Technical Memorandum |
| 12. Sponsoring Agency Name and Address<br>National Aeronautics and Space Administration<br>Washington, D.C. 20546 | | |
| | | 14. Sponsoring Agency Code |

15. Supplementary Notes

16. Abstract

Noise data were obtained with a large-scale cold-flow model of a two-flap, under-the-wing, externally blown flap proposed for use on future STOL aircraft. The noise suppression effectiveness of locating a slot nozzle at the trailing edge of the second flap and of applying partial covers to the slots between the wing and flaps was evaluated. Overall-sound-pressure-level reductions of 5 dB occurred below the wing in the flyover plane. Existing models of several noise sources were applied to the test results. The resulting analytical relation compared favorably with the test data.

| 17. Key Words (Suggested by Author(s))<br>Jet noise; STOL aircraft noise; EBF noise;<br>Impingement noise; Jet flap noise | 18. Distribution Statement<br>Unclassified - unlimited<br>STAR category 71 | |
|---|---|---|
| 19. Security Classif. (of this report)<br>Unclassified | 20. Security Classif. (of this page)<br>Unclassified | 21. No. of Pages<br>64 |  22. Price*<br>$4.25 |

# NOISE REDUCTION TESTS OF LARGE-SCALE-MODEL EXTERNALLY BLOWN

# FLAP USING TRAILING-EDGE BLOWING AND

# PARTIAL FLAP SLOT COVERING

by Daniel J. McKinzie, Jr.; Robert J. Burns; and Jack M. Wagner

Lewis Research Center

## SUMMARY

Noise data were obtained with a large-scale cold-flow model of a two-flap, under-the-wing, externally blown flap being investigated for STOL aircraft. The wing and flap were positioned in the approach configuration, referred to in this report as the baseline configuration. The study evaluated the noise suppression effectiveness of, first, locating a slot nozzle at the trailing edge of the second flap through which secondary air is blown; second, applying partial spanwise covers to the slots between the wing and flaps; and third, the combination of these two devices.

The largest noise reductions were obtained for the baseline configuration with slot nozzle blowing and partial covering of the slots between the wing and flaps. Overall-sound-pressure-level noise reductions of 4.5 decibels occurred in the forward quadrant below the conical nozzle and flaps, in the flyover plane. A maximum noise reduction of 5 decibels occurred directly below the nozzle and flaps at a jet Mach number of 0.5 and decreased with increasing jet velocity.

Several existing noise source models were applied to the test results of the baseline configuration. The resulting analytical relation compared favorably with the test data in magnitude and trend at jet Mach numbers between 0.5 and 0.8. An analysis of the noise source mechanisms shows that the dominant noise appears to emanate from three principal sources: first, the impact of the jet on the surface of the second flap; second, a fluctuating lift response to an upwash disturbance produced by the inflow of the jet exhaust about the wing and flaps; and third, the flow over the trailing edge of the second flap. The use of the suppression devices described in this report did not affect the impact source of noise, which the present analysis indicates produces the dominant noise directly beneath the nozzle and wing.

# INTRODUCTION

The engine exhaust of the under-the-wing (UTW) externally blown flap (EBF) short takeoff and landing (STOL) aircraft is deflected downward by the flaps of the wing during takeoff and approach (fig. 1). Noise levels from 10 to 18 decibels greater than the jet noise are generated by the impingement of the jet on the flap surfaces (refs. 1 and 2).

NASA has conducted experimental research and development work to measure and define the flap interaction noise field for a variety of UTW configurations, as discussed in reference 3. The configurations included large- and small-scale models of a conical nozzle with a curved or slotless wing, a two-flap wing, and a three-flap wing. Other types of nozzles used included mixer nozzles and coannular nozzles, which produce large velocity decay rates. The small models initially provided screening information to the program and together with the large models provided the data base for correlation and scaling laws.

These studies established a need for noise suppression techniques to meet the proposed noise goal of 95 effective preceived noise decibels (EPNdB) at a 152.4-meter (500-ft) sideline for powered lift aircraft (ref. 1). These studies also identified several specific noise sources. The sources included flap leading-edge noise, scrubbing noise, and trailing-edge noise, with the latter hypothesized as being most probably dominant. In addition to these, reference 4 speculates that the large-scale turbulence structures of the jet flowing downstream from the nozzle exit produce unsteady inflow in the vicinity of the flaps. This flow causes a fluctuating lift response, which might produce noise.

Concepts proposed to suppress trailing-edge noise generally use devices located on or in the vicinity of the flap surfaces. These devices include both the active blowing of low-speed air through a slot located near the trailing edge of a flap (refs. 5 to 7) and the use of perforated panels and screens positioned in or on the flap surfaces. These devices appear to react with the passing flow field to change the effective impedance of the surfaces (refs. 8 to 10).

The primary objective of this study, conducted at the NASA Lewis Research Center, was to evaluate experimentally the noise suppression effectiveness of the following: first, locating a slot nozzle, through which secondary air is blown, at the trailing edge of the second flap; second, partially covering the spanwise slots between the wing and flaps; and third, the combination of these two noise suppression devices.

A 33-centimeter-diameter conical nozzle simulating a jet engine nozzle but using cold flow was tested with a wing model having a chord length, with flaps retracted, of 2.13 meters. Acoustic data were taken in the plane of the nozzle axis, perpendicular to the wing. The model configuration simulated a two-flap wing EBF approach configuration, which produces greater noise than the takeoff configuration (ref. 11). This model configuration is referred to in this report as the baseline configuration.

A second objective was to evaluate several noise source models used to predict the test results of the baseline configuration. These models include estimates of the overall sound pressure level for trailing-edge noise, impact noise (as defined in ref. 4), and the noise resulting from jet inflow about the wing and flaps. A theoretical approach for the calculation of trailing-edge noise is briefly discussed in this report along with an empirical method, first presented in reference 4, for determining impact noise. Also, a theoretical approach for calculating the noise resulting from jet inflow is discussed. These approaches are then combined to provide an estimate of the overall sound pressure level of impingement noise for the baseline configuration. The calculated noise estimates are finally compared with the measured noise levels. The noise source models are also applied to the configurations other than the baseline configuration in order to aid in understanding the noise source reductions in the treated configurations.


## APPARATUS AND PROCEDURE


### Test Facility


The cold-flow externally blown flap tests were conducted at the large-scale test facility schematically shown in figure 2. A primary airflow system supplied air to the large 33-centimeter-diameter conical nozzle, and a secondary system supplied air to the slot nozzle located at the trailing edge of the second flap.

Primary airflow system. - The primary airflow system to the 33-centimeter-diameter nozzle is shown in figure 2. The nozzle centerline is 3.89 meters above grade. Dry, ambient temperature air is supplied to a 41-centimeter-diameter gate shutoff valve through a 61-centimeter-diameter underground pipeline from the air supply system at about 1000 kilonewtons per square meter. Flow rate and nozzle pressures are set by adjustment of a 25.4-centimeter-diameter butterfly control valve. An orifice flowmeter is located in the underground line upstream of the shutoff valve.

A muffler system in the line downstream of the control valve attenuates internal noise, caused primarily by the control valve. Essentially, the muffler system consists of perforated plates and two dissipative mufflers. The perforated plates (40 percent open area) are located downstream of and adjacent to the control valve. The mufflers are sections of pipe containing two splitter plates oriented at right angles, so that the flow is divided into four channels. All internal surfaces of the mufflers are covered with acoustic absorbent material. The second muffler is located downstream of the last 45° elbow to take advantage of the reflections caused by turning the flow. In addition, the flow line is wrapped with fiberglass and leaded vinyl sheet to impede direct radiation of noise through the pipe wall. Two screens are placed in the air line down-

stream of the last muffler to improve the uniformity of the flow to the nozzle.

Secondary airflow system. - The airflow system which supplied air to the slot nozzle located on the trailing edge of the second flap is shown in figure 3. The air supply was tapped from the primary flow system at a point downstream of the butterfly control valve. A manually operated gate control valve and a flowmeter run were located downstream of the tapoff point. A perforated plate and two in-line mufflers were located downstream of the flowmeter run. The internal surfaces of the mufflers were covered with acoustic absorbent material.

Aerodynamic instrumentation. - Four 12-tube boundary-layer rakes were used to obtain velocity profile data at the trailing edge of the second flap of the baseline configuration. One rake was located at a point along the trailing edge referred to as the centerline point. This point was located where a plane perpendicular to the impact surface of the flap intersected the axis of the conical nozzle and the trailing edge of the flap. The remaining rakes were located at spanwise stations 15.2, 30.5, and 45.7 centimeters from the centerline point.

A static-pressure distribution around the chord of the second flap was obtained in the plane of the centerline point by using two 10-tube (0.397-cm o.d., 0.238-cm i.d.) plastic belts bonded to the surface of the flap. Nineteen static-pressure taps were distributed around the flap as shown in figure 4.

Acoustic instrumentation. - The microphone circle is shown in figure 5. Twenty microphones were placed on a 15.24-meter-radius circle over a smooth blacktop ground plane. Noise measurements were made with 1.27-centimeter-diameter condenser microphones. The noise data were analyzed by a one-third-octave-band spectrum analyzer which determined sound-pressure-level spectra referenced to 20 micronewtons per square meter.


Model Configurations


Four wing-flap configurations were tested by using the 33-centimeter-diameter conical nozzle with the wing mounted vertically (fig. 2). The model wing had a 2.13-meter chord with the flaps retracted and a 2.74-meter span. The wing was configured to represent the STOL approach condition with the first and second flap chord lines oriented at $30^O$ and $60^O$, respectively, to the wing chord line as shown in figure 6. The four configurations were designated as follows: first, the baseline configuration (reference configuration); second, the baseline configuration with plugs; third, the baseline configuration with slot nozzle blowing; and fourth, the baseline configuration with the combination of plugs and slot nozzle blowing. The plugs were partial spanwise covers applied over the slots between the wing and the first flap and between the first and

4

second flaps when the flaps were deployed (see fig. 7). These covers were smooth fairings positioned on the flaps and centrally located in relation to the intersection of the nozzle axis with the flaps. They were designed to prevent most of the impinging jet flow from passing through the spaces between the wing and the flaps. Thus, they redirected this flow over and downstream on the impingement side of the flaps. The slot nozzle located at the trailing edge of the second flap is shown in figures 3 and 8.

The slot nozzle was centrally located on the trailing edge of the second flap in relation to the axis of the conical nozzle. The secondary air system supplied sufficient air to the slot nozzle so that Mach numbers up to 0.5 could be achieved. As noted in figure 8, air entered opposite ends of the second flap through diffuser couplings and passed into a plenum chamber integrally formed to the flap profile. After mixing in the plenum, the air passed through a perforated orifice plate having 1.27-centimeter-diameter holes and a porosity of 45 percent. It then entered a second settling chamber before passing through a second perforated orifice plate having 0.64-centimeter-diameter orifices and a porosity of 45 percent. From the second orifice plate the air entered an acceleration section leading to the trailing edge of the flap. This section consisted of six adjacent 30.5-centimeter spanwise compartments separated from each other by side plates. For the tests described in this report four of these sections were used so that the slot nozzle had a slot height of 2.54 centimeters and an overall length of 122 centimeters. The location of the slot nozzle at the trailing edge of the second flap and the choice of slot nozzle velocities were based, in part, on results obtained from the small-scale tests reported in reference 7.


Procedure


The slot nozzle and the conical nozzle exhaust velocities were calculated from the isentropic gas dynamic equations, in which fully expanded flow was assumed. Stagnation temperatures ranged between 280 and 289 K. For the configurations using slot nozzle blowing, the slot nozzle was operated at a nominal slot Mach number $M_{slot}$ of 0.4. (Symbols are defined in appendix A.)

Noise measurements were made at nominal values of jet Mach number $M_j$ of 0.5, 0.7, and 0.8. To minimize the effect of ground reflections data were taken with 20 microphones located first at 0.10 meter and then at 3.58 meters above the ground plane. The sound-pressure-level SPL data taken at 3.58 meters were combined at approximately 2 kilohertz with the data taken at 0.10 meter. This was done by correcting the 0.10-meter data to 3.58 meters above the ground plane by using the spectral reflectance corrections presented in figure 9, which were calculated by using reference 12 and assuming a point source. Thus, the final spectral data are 2.55 decibels above the free

field (as though they were taken at a height of 3.58 m above a hard smooth surface free from discrete ground effects). An exception to this occurred in the case of the baseline configuration with plugs and slot nozzle blowing, where the noise measurements were simultaneously taken at 0.10 and 3.58 meters above the ground plane (i.e., 10 microphones at each height).

Three samples of acoustic data were taken at each microphone, averaged, and corrected for atmospheric attenuation by the method of reference 13 to give lossless sound-pressure-level data.

## ANALYSES OF JET-FLAP-INTERACTION NOISE

One of the objectives of this report is to apply several noise source models to the test results, in particular, results for the baseline configuration. The models include overall-sound-pressure-level OASPL estimates of trailing-edge noise; the noise resulting from inflow about the wing and flaps, referred to in this report as inflow noise; and impact noise.

Figure 10(a) depicts jet impingement of an EBF two-flap wing in its approach configuration. Regions $A_1$, $A_2$, and $A_3$ (as defined in ref. 4) represent locations of the major noise sources: $A_1$ is a spherical region enclosing the impingement zone; $A_2$ is a conical region enclosing the upstream wall jet; and $A_3$ is a spherical region enclosing the downstream wall jet and the flow fields at the trailing edge and suction side of the second flap. In figure 10(b) the major noise sources are assumed to be the result of oblique jet impingement, surface scrubbing, jet interaction with the leading and trailing edges, free shear-layer mixing over the surface of the deflected flap, and inflow about the second flap.

In reference 4 it is indicated that the noise resulting from oblique jet impingement, surface scrubbing, and free shear layer mixing, located within region $A_1$ of figure 10(b), is approximated by impact noise. Impact noise $OASPL_{impact}$ is defined as all the noise produced on a flat surface sufficiently large to exclude leading- and trailing-edge noise. The noise produced by inflow about the wing or flaps is referred to in this report as inflow noise. Leading-edge noise is not considered in this report because in reference 14 it is reported to be less than trailing-edge noise. Thus, it is assumed that trailing-edge noise, impact noise, and inflow noise are dominant. By assuming that the sound sources are uncorrelated, as proposed in references 4 and 15, one may approximate their combined sound field by superposition. Therefore, the total OASPL is expressed as the logarithmic sum of impact, trailing-edge, and inflow OASPL:

6

$$\text{OASPL}_{\text{impinge}} = 10 \log \left[ 10 \exp \left( \frac{\text{OASPL}_{\text{impact}}}{10} \right) + 10 \exp \left( \frac{\text{OASPL}_{\text{TE}}}{10} \right) \right.$$

$$\left. + 10 \exp \left( \frac{\text{OASPL}_{\text{inflow}}}{10} \right) \right] \quad (1)$$

This summation is referred to in this report as impingement noise. The following sections present analytical expressions in SI units used to estimate trailing-edge, inflow, and impact noise.

## Trailing-Edge Noise

Edge noise was analyzed in reference 16 and shown to have a velocity dependence of $U^5$. In the work of reference 17 edge noise was studied empirically and was concluded to have a velocity dependence of $U^6$. In the study of reference 18 the low Mach number data of reference 17 were reexamined and shown more closely dependent on $U^5$. Therefore, trailing-edge noise is estimated in this report from the theoretical approach of reference 16 in the form presented in equation (11) of reference 4. Details of the derivation are presented in reference 4; hence, only a brief review of its mathematical expression is given in this section.

It is assumed that a directed flow lies on the surface of a semi-infinite plane which is thin and rigid (see fig. 11, taken from ref. 4). The phenomena of interest occur near or at the edge of the half-plane. Eddies in the flow are well within a wavelength of the edge. The observer is assumed to be in the far field, and the flow region is turbulent and at high Reynolds number. In figure 11, $\delta$ represents the thickness of the boundary layer; W is taken as the spanwise length of the velocity profile between the centerline and a point where the local velocity is equal to one-half the maximum velocity $U_m$ of the free shear layer at the trailing edge; r is the distance to the observer measured from the trailing edge of the half-plane; and the angles $\psi$ and $\varphi$ locate, in cylindrical coordinates, the field point referenced to the edge of the plate.

The expression for trailing-edge noise is derived from Lighthill's analysis, in which the turbulence is divided into regions of perfect correlation where the size of each region is very much less than the acoustic wavelength. From these considerations, the overall sound pressure level of trailing-edge noise $\text{OASPL}_{\text{TE}}$ is given by equation (11) of reference 4 as follows:

$$\text{OASPL}_{\text{TE}} = 10 \log \frac{W\delta U_m^5}{r^2} + 10 \log \cos^2 \frac{\psi}{2} + 10 \log \frac{1.15 \times 10^6 \rho^2}{c} \qquad (2)$$

(see fig. 11 for the coordinate system). The angle $\psi$ was determined graphically as a function of the acoustic radiation angle $\theta$. It may, however, be crudely approximated by setting

$$\psi \approx 60^{\text{O}} + \theta$$

The constant in the last term of equation (2) includes the normalized turbulence intensity, which is assumed in this analysis to have a magnitude of 0.1.

## Inflow Noise

A derivation of the noise produced from inflow effects is given in appendix B. The derivation is based on reference 17, in which an estimate of the dipole noise is presented for cases in which the source is considered intermediate between satisfying the conditions for compactness and noncompactness. One of the primary assumptions made in the derivation in this report is that the large-scale turbulence structures of the nozzle flow field (ring vortices) are responsible for what is referred to as inflow noise. It is speculated in reference 4 that these structures could interact with the flaps of the UTW EBF in an aerodynamic sense and result in unsteady inflow about the flaps. This in turn could cause a fluctuating lift response, which would have an influence on the production of noise. This speculation is, in part, based on observations made of the large-scale turbulence structures in reference 19, which are more fully discussed in appendix B.

The analysis of reference 17 considers a rigid airfoil immersed in a subsonic turbulent inflow. For the special case when the characteristic size of the eddies is not small with respect to the chord length of the airfoil, it is suggested that an application may be made of some form of quasi-steady solution describing the lift fluctuations. Once the lift fluctuations are described, the surface may be modeled as a small (i.e., small with respect to a wavelength) spherical source, and the point dipole expression may be modified to account for reduced radiation at acoustic wavelength body size ratios which are small with respect to the chord. From these considerations the overall sound pressure level of inflow noise $\text{OASPL}_{\text{inflow}}$, derived in appendix B, is given as follows:

$$OASPL_{inflow} = 10 \log \left[ \frac{\left(C_L\right)_\alpha \rho_l U_l^2}{r} \right]^2 + 10 \log \left( A_c \frac{A}{A_c} \right) + 10 \log \left[ \frac{A}{A_c} \left( \frac{\pi}{\frac{7.559}{M_l^2} + 1} \right) \right]$$

$$+ 10 \log \left( \frac{\frac{v'}{U_l}}{8\pi P_{ref}} \right)^2 + 10 \log \cos^2 \beta + 10 \log (0.23 \, f_r) \qquad (3)$$

### Impact Noise

Although the specific mechanism which produces impact noise is not known, it is indicated in reference 4 that the large-scale turbulence structures present in the jet flow field may be involved. Therefore, the assumption is made in this analysis that impact noise is produced, in part, by the large-scale structures of the jet flow field impacting the flaps.

In the absence of an explicit theoretical expression for impact noise, it is proposed, as in reference 4, that the small-scale test results of reference 20 be used to estimate it. In reference 20 the noise field produced when a 5.2-centimeter-diameter jet impacted a very large smooth flat board is presented. The noise field did not include leading- and trailing-edge noise, but did include the remaining noise sources (i.e., oblique jet impingement coupled with surface viscosity effects, surface scrubbing, reflection by the surface, free jet mixing, and free shear-layer mixing over the deflected flat surface). The large-flat-board tests were made to investigate the acoustic effects produced by changes in the separation distance between the nozzle exit plane and the board, by changes in the angle of incidence between the nozzle axis and the plane of the board, and by a range of subsonic and low supersonic Mach numbers. These conditions included nondimensional geometric and fluid flow conditions similar to those of the tests described in this report. The data of reference 20, however, are corrected for differences in nozzle diameter $D$ and microphone location $r$ according to the scaling laws presented in reference 21 as follows:

$$OASPL_2 - OASPL_1 = 10 \log \left[ \left( \frac{D_2}{D_1} \right)^2 \left( \frac{r_1}{r_2} \right)^2 \right] \qquad (4)$$

9

The test results of reference 20 are shown in figure 12 and were used after interpolation for the present nozzle flow velocity conditions.

## EXPERIMENTAL RESULTS

The following discussion is divided into two parts. The first part consists of the presentation of noise data for the baseline configuration in the approach configuration (overall flap deflection angle, $60^O$). The second part presents a comparison between the noise produced by the baseline configuration (reference condition) and the three configurations employing noise suppression devices. The devices include trailing-edge blowing, plugs in the slots between the flaps, and a combination of these two devices.

During approach ($2^O$ angle of attack of the wing chord, ref. 22) the portion of the aircraft noise footprint of particular interest lies between values of the radiation angle $\theta$ of $70^O$ and $100^O$. Thus, for the configurations in which the suppression devices are used, the data for $\theta$ between $10^O$ and $115^O$ are presented. However, the OASPL and spectral data for $\theta$ between $10^O$ and $350^O$ are included for the baseline configuration, which is a primary configuration of the EBF. Included in these additional data are free field spectral data which have not been presented previously. These data are necessary in order to understand the noise source mechanisms.

### Baseline Configuration

The discussion of the baseline configuration is divided into two parts. The first part considers the OASPL directivity data, and the second considers the SPL spectra.

Overall-sound-pressure-level directivity. - The OASPL distributions between values of the radiation angle $\theta$ of $10^O$ and $350^O$ are presented in figure 13 at values of the nozzle exit Mach number $M_j$ of 0.5, 0.7, and 0.8. The data show similar changes in OASPL with radiation angle as a function of $M_j$ for $10^O \leq \theta \leq 70^O$ and for $200^O \leq \theta \leq 350^O$. However, between $70^O \leq \theta \leq 115^O$ and $155^O \leq \theta \leq 200^O$ there is a disproportionate increase in noise level with increased jet exit Mach number $M_j$. The increase in noise level between $\theta = 70^O$ and $115^O$ may indicate that a sound source having a greater dependence on jet velocity is acting directly below the aircraft, at $\theta = 87^O$, which is within the range of particular interest between $\theta = 70^O$ and $100^O$.

Sound-pressure-level spectra. - The spectra for the baseline configuration are presented in figure 14. These data demonstrate the distinct broadband character of the sound field as a function of the radiation angle $\theta$ and the jet exit Mach number $M_j$.

In the high-frequency range between 3.15 and 20 kilohertz the data have similar

slopes (6 dB per octave) throughout the microphone circle with exceptions at $\theta = 270^O$ and $290^O$. At these angles the data show a distinct reduction in slope and a rise in the average sound pressure level. Thus, a high-frequency noise source was radiating within a narrow angular range of approximately $20^O$ almost directly over the wing of the baseline configuration.

Between $\theta = 185^O$ and $290^O$ (figs. 14(j) to (p)) two broadband peaks in the spectra occur at $M_j = 0.7$ and $0.8$. These two peaks are similar to the two peaks discussed in reference 23. The upper, more blunted peak centers around a frequency of 1.6 kilohertz, and the lower peak occurs at approximately 315 hertz.

In the low-frequency range between 50 and 250 hertz the greatest changes in the slopes and levels of the data occur. For example, between $\theta = 10^O$ and $100^O$ (figs. 14(a) to (f)) a steady decrease in SPL with increasing $\theta$ is clearly noted at all values of $M_j$.

The frequencies at which the peak values of SPL occur change as functions of radiation angle $\theta$ and jet exit Mach number $M_j$. For example, at $M_j = 0.5$ and $\theta = 10^O$ and $25^O$ the peak SPL occur near 125 hertz. Between $\theta = 55^O$ and $70^O$ two dominant peaks occur at 100 and 250 hertz, and between $\theta = 85^O$ and $115^O$ single broad peaks occur near 250 hertz. These broad peaks comprise a peak at 200 hertz and either or both of the peaks near 100 and 315 hertz. At $M_j = 0.7$ and $0.8$ between $\theta = 10^O$ and $215^O$ (figs. 14(a) to ($l$)) a dominant peak in SPL occurs at approximately 315 hertz, while between $\theta = 10^O$ and $70^O$ a lesser second peak occurs between 100 and 125 hertz.

It is important to note that the nature of the high- and low-frequency noise spectra revealed here would have been less clear if the technique of taking noise data at 0.10 and 3.58 meters above the ground plane had not been used.

<u>Turbulent modal forms</u>. - In figures 14(a) to (g), between $\theta = 10^O$ and $115^O$, three tick marks are distributed along each curve. These tick marks represent the frequencies at which several modal forms of the large-scale turbulence structures in a jet flow field are predicted to occur (ref. 19). The tick mark labeled ① represents the experimentally based fundamental axisymmetric vortex mode (applicable at $M_j < 0.85$). The tick mark labeled ② represents the first harmonic of the axisymmetric vortex mode. The tick mark labeled ③ represents the planar-parallel-flow boundary-layer instability mode. The parameters upon which these modes depend are presented in reference 4.

The possibility that the large-scale turbulence structures in a jet flow field are associated (through transfer functions) with the dominant noise produced during jet impingement with a flat plate is considered in reference 4. It is shown that the first harmonic mode of these structures occurs at approximately the same frequency as the peak value of the sound spectra.

In figures 14(a) to (g) either tick mark ① (at $M_j = 0.5$) or tick mark ② (at $M_j = 0.5, 0.7,$ and $0.8$) coincides with the peak value of the spectra. Thus, as with the flat plate data of reference 4, these data show that either of these vortex modes occurs at

approximately the same frequency as the peak value of the spectra. Thus, it appears that the large-scale turbulence structures in the jet flow field are associated with the dominant noise produced during jet impingement with the flaps.

## Overall-Sound-Pressure-Level Comparisons Between Baseline

## and Suppressed Configurations

Comparisons are presented in this section between the OASPL data of the baseline configuration and the three configurations modified with the suppression devices.

Slot nozzle blowing. - The results for the baseline configuration with slot nozzle blowing at the trailing edge of the second flap are presented in figure 15. Also shown, for comparison, is the OASPL distribution for the slot nozzle alone operating at its maximum flow velocity of 142 meters per second. The data show that no reduction in OASPL occurred because of slot blowing. (The slot flow velocity was constant at 142 m/sec over the center length of 61 cm and decreased to 131 m/sec for a distance of 30.5 cm on either side of this section. And the background noise was negligible in comparison with that of the slot nozzle alone.)

Plugs in slots. - A comparison is presented in figure 16 between the OASPL of the baseline configuration and the baseline configuration with plugs. Reductions of at least 2.0 decibels occurred at all test conditions between $25^O$ and $85^O$. The largest noise reduction between $85^O$ and $115^O$ occurred at $M_j = 0.5$ and amounted to 4 decibels.

Plugs and slot nozzle blowing. - The OASPL of the baseline configuration and a limited amount of data for the baseline configuration with plugs and slot nozzle blowing are compared in figure 17. Noise reductions of approximately 4.5 decibels were produced between $40^O$ and $55^O$, where data were available. The largest reduction at $85^O$ occurred at $M_j = 0.5$ and amounted to 5 decibels.

Effectiveness of suppression devices. - When the results presented in figures 15 to 17 are compared, several observations may be made: first, the largest noise reductions (up to 5 dB) occurred for the baseline configuration with plugs and slot nozzle blowing; second, slot nozzle blowing by itself was ineffective as a suppression device; and third, at $\theta = 85^O$ the suppression devices used in this study were not equally effective in reducing the noise at all jet Mach numbers, that is, the largest noise reductions occurred at the lowest $M_j$, 0.5.

## Spectral Comparisons Between Baseline and Suppressed Configurations

The spectra of the three configurations with suppression devices are shown in figures 18 to 25. Also shown for comparison are the spectra of the baseline configuration.

Only a limited amount of data was obtained over the full frequency range for the baseline configuration with plugs and slot nozzle blowing; these data are presented in figures 20, 21, and 23 at $\theta = 40^O$, $55^O$, and $85^O$, respectively. In addition, data for this configuration over the limited frequency range 1.6 to 20 kilohertz are included in figures 18, 22, and 24 at $\theta = 10^O$, $70^O$, and $100^O$, respectively. These data are limited to this frequency range because the complementary acoustic data normally taken at 0.10 meter above the ground plane were not obtained at these radiation angles. For the baseline configuration with plugs the data obtained at $\theta = 40^O$ (fig. 20) are limited to the frequency range 50 to 1250 hertz because the microphone used to obtain the complementary data at 3.58 meters above the ground plane malfunctioned.

High-frequency (6.3- to 20-kHz) spectra. - At frequencies between 6.3 and 20 kilohertz each of the configurations having suppression devices except one produced as much or more noise than the baseline configuration. The exception is the baseline configuration with plugs and slot nozzle blowing, which produced a slight noise reduction at $\theta = 85^O$ for $M_j = 0.7$ and 0.8 (figs. 23(b) and (c), respectively). At $M_j = 0.5$ slot nozzle blowing produced a rise in SPL between 1.6 and 20 kilohertz for the two configurations in which it was used. This effect is believed due to the high-frequency noise produced by the slot nozzle alone. Results for the slot nozzle alone are shown in figure 26 for radiation angles of $40^O$, $55^O$, and $85^O$. These broadband spectra peak in the vicinity of 2.5 kilohertz. At the higher jet Mach numbers of 0.7 and 0.8 slot nozzle noise also appears in the data of the baseline configuration with plugs and slot nozzle blowing at $\theta = 40^O$, $55^O$, and $85^O$ in figures 20, 21, and 23, respectively.

Midfrequency (250- to 1600-Hz) spectra. - In the frequency range between 250 and 1600 hertz significant noise suppression occurred for the two configurations in which plugs were used. Specifically, at $\theta = 40^O$ and $55^O$ in figures 20 and 21, respectively, reductions amount to from 5 to 12 decibels. Also reductions from 5 to 9 decibels were obtained at $85^O$, as noted in figure 23. Figures 19 to 21, 23, and 24 indicate that the use of plugs produced a noise reduction in the 315- and 400-hertz bands; this reduction may have been the result of a decrease of the inflow of the large orderly turbulence structures about the flaps.

Low-frequency (50- to 160-Hz) spectra. - In the low-frequency range between 50 and 160 hertz and for $10^O \leq \theta \leq 55^O$ (figs. 18 to 21) only a small noise reduction occurred for the two configurations in which plugs were used.

Most effective suppression devices. - The use of the plugs and slot nozzle blowing produced the largest noise reductions in midfrequencies (250 to 1600 Hz) between $\theta = 40^O$ and $85^O$. Also reductions in the high-frequency range (1.6 to 10 kHz) occurred at $\theta = 85^O$ and $M_j = 0.7$ and 0.8. In the low-frequency range (50 to 160 Hz) small noise reductions occurred between $\theta = 10^O$ and $55^O$.

## Velocity Exponent Directivity

In figures 27 to 30 distributions are presented of the jet-flap interaction velocity exponent $N$ that were determined from slopes constructed tangent to the curves of $\sum$ SPL plotted as a function of the jet impingement velocity $U_i$. Each $\sum$ SPL was evaluated in the same manner as OASPL, but over a reduced range of frequencies, and $U_i$ was determined from a jet velocity decay relation, presented in reference 24, for a single jet and was evaluated at a point 7.33 nozzle diameters downstream of the nozzle exit plane. These plots are shown for the baseline configuration and the three configurations modified with suppression devices between $\theta = 10^O$ and $115^O$. The figures are presented as an aid in showing the noise source distribution and the effect of jet Mach number $M_j$ on that distribution. Each figure includes two distributions based on two different sets of $\sum$ SPL data. One set was computed by using a range of low-frequency spectra from 50 to 800 hertz, and the other set was computed by using a range of high-frequency spectra from 3.15 to 20 kilohertz. These two ranges were chosen to demonstrate further the character of the noise sources as a function of frequency. Since the velocity exponents were determined from curves based on only three-point velocity data, some caution should be taken in interpreting their absolute values.

Baseline configuration. - A distribution of $N$ as a function of $\theta$ is presented in figure 27 for the baseline configuration. Between $\theta = 10^O$ and $70^O$ the magnitude of the low-frequency-based $N$ (fig. 27(a)) at all three values of $M_j$ has a nominal value of 5.5. For $\theta > 70^O$ the exponent increases sharply at $M_j = 0.7$ and 0.8 while remaining nominally at 5 for $M_j = 0.5$. These data indicate that a second sound source may be dominant at $\theta > 70^O$ and that it increases in dominance at $M_j > 0.5$.

The high-frequency-based values of $N$ shown in figure 27(b) have a nominally constant value of 9 between $\theta = 40^O$ and $115^O$ and are thus independent of jet velocity. Between $10^O$ and $25^O$, however, they are strongly dependent on jet velocity.

Slot nozzle blowing. - As shown in figure 28, the high-frequency-based values of $N$ for the baseline configuration with slot nozzle blowing are dependent on jet velocity, but are nominally independent of $\theta$ at $M_j = 0.7$ and 0.8. At $M_j = 0.5$, however, the exponent increases between $\theta = 70^O$ and $115^O$ and has a smaller value than that shown in figure 27(b) for the baseline configuration. The low-frequency-based data are the same as those of the baseline configuration (fig. 27(a)).

Most of the noise generated by the slot nozzle alone occurs between frequencies of 2.5 and 20 kilohertz, as shown in figure 26, which includes the range of spectral data used to determine the high-frequency-based $N$ for the baseline configuration with slot nozzle blowing. Therefore, the large differences in $N$ between figures 27(b) (baseline configuration) and 28 are believed due to the high-frequency noise generated by the slot nozzle flow interacting in crossflow with the conical nozzle flow as it passed over the

second flap and its trailing edge.

Plugs in slots. - The distributions of N for the baseline configuration with plugs are presented in figure 29. The magnitudes of N are similar to those shown in figure 27 for the baseline configuration, but the distributions with $\theta$ are slightly different.

Plugs and slot nozzle blowing. - The distributions of N for the baseline configuration with plugs and slot nozzle blowing are presented in figure 30. Though the low-frequency-based N data at $M_j$ = 0.7 and 0.8 are limited, the magnitudes are generally larger than those for the baseline configuration with plugs. However, at $M_j$ = 0.5 the data show some similarity in both distribution with $\theta$ and magnitude to the baseline configuration with plugs (fig. 29(a)).

The high-frequency-based N data are similar to those of the baseline configuration with slot nozzle blowing (fig. 28) in that N is strongly dependent on jet velocity. These data are believed to be the result of the high-frequency noise generated by the slot nozzle flow interacting in crossflow with the conical nozzle flow as it passed over the second flap and its trailing edge.


## COMPARISON OF CALCULATED AND MEASURED JET-FLAP INTERACTION NOISE

In this section the experimental data are compared with calculated estimates of the noise for the baseline configuration, the baseline configuration with plugs, and the baseline configuration with plugs and slot nozzle blowing. A comparison of the baseline configuration with slot nozzle blowing is not made because its OASPL distribution is similar in magnitude to that of the baseline configuration. The principal reason for making these comparisons, in the cases of the configurations having suppression devices, is to aid in understanding the noise source mechanisms acting in the baseline configuration.

The noise source models combined to obtain an estimate of the overall noise levels are trailing-edge noise, inflow noise, and impact noise. Trailing-edge noise is calculated by using equation (2), where the boundary-layer height $\delta$ and spanwise wetted edge 2W are evaluated at the trailing edge of the second flap. These quantities are presented in figures 31 and 32, respectively. The velocity profiles showing the boundary layer were determined at the centerline point on the trailing edge of the flap, and the spanwise velocity profiles were taken at an arbitrary height of 3 centimeters above the impact surface (beyond the boundary-layer height in the plane of the trailing edge). A static surface pressure distribution, obtained in the plane of the chord and centerline point of the flap, is presented in figure 33 in terms of the pressure coefficient $C_p$. The $C_p$ distribution shows that the flow about the second flap was attached. Inflow noise is calculated by using equation (3), in which the large-scale turbulence structures are assumed to inflow about the wing and flaps. The slope of the lift coefficient $\left(C_L\right)_\alpha$ in

equation (3) is estimated by using equation (B14). Impact noise is estimated from the experimental data of reference 20. The estimates of trailing-edge and inflow noise must be corrected from the free field to a point 3.58 meters above the ground plane, while impact noise does not require this correction.

The measured data of the baseline configuration are compared with an estimate of the total noise $\text{OASPL}_{\text{impinge}}$, where the total noise is calculated by logarithmically summing trailing-edge noise, impact noise, and inflow noise according to equation (1).

The measured data of the baseline configuration with plugs are compared with the logarithmic sum of trailing-edge noise (eq. (2)) and impact noise $\text{OASPL}_{\text{impact, TE}}$; the result is expressed by the following equation:

$$\text{OASPL}_{\text{impact, TE}} = 10 \log \left[ 10 \exp \left( \frac{\text{OASPL}_{\text{impact}}}{10} \right) + 10 \exp \left( \frac{\text{OASPL}_{\text{TE}}}{10} \right) \right] \qquad (5)$$

The measured data of the baseline configuration with plugs and slot nozzle blowing are compared with the estimate of impact noise from the experimental data of reference 20.

The calculated OASPL distributions (eq. (1), eq. (5), or impact noise) are compared with the test results in figures 34 to 36 between $\theta = 10^{\circ}$ and $120^{\circ}$ at $M_j = 0.5$, 0.7, and 0.8. The curves are restricted to this range of $\theta$ because of the limits of the useful large-flat-board data (ref. 20) representing impact noise. The distribution of the velocity exponent $N$ is shown in the lower portion of the figures. The OASPL data used to determine the velocity exponents were calculated from spectral data between 50 hertz and 20 kilohertz.

Baseline Configuration

The baseline configuration OASPL distributions are presented in figure 34. Included are the theoretical estimates of trailing-edge noise (eq. (2)) and inflow noise (eq. (3)) applied to the wing and both flaps, the empirical estimate of impact noise, and the impingement noise as defined by equation (1).

A comparison of the calculated curves in figure 34 representing trailing-edge noise (eq. (2)) and the measured data shows that the measured data are from 7 to 15 decibels greater than the calculated values at all values of jet Mach number $M_j$. Therefore, edge noise as predicted by equation (2) cannot be considered the dominant source of noise between $\theta = 25^{\circ}$ and $120^{\circ}$. Figure 34 also indicates that, as $M_j$ increases, impact and inflow noise become increasingly dominant in relation to edge noise.

At $M_j$ = 0.5 (fig. 34(a)) the calculated impingement noise ($OASPL_{impinge}$, eq. (1)) is generally 1.5 decibels below the measured data between $\theta$ = 40° and 85°. This may be due to a low estimate of impact noise which is based on the scaled-up test results of reference 20. In the lower portion of figure 34(a) the velocity exponents determined from experimental data result in a nominal velocity dependence of $U^5$ throughout the range of $\theta$ between 10° and 115°. This agrees generally with the expected distribution based on equation (1) except in the region between $\theta$ = 90° and 120°, where impact noise, having a velocity dependence of $U^8$, appears to be dominant. This disagreement between $\theta$ = 90° and 120° may be due to the limited amount of test data taken and used to determine the velocity exponents and the fact that the test data at $M_j$ = 0.5 are the lower limit of that data. Therefore, the velocity exponents determined at $M_j$ = 0.5 may be less accurate than those determined, for example, at $M_j$ = 0.7.

Figures 34(b) and (c) present the measured data and curves representing impingement noise at jet Mach numbers of 0.7 and 0.8, where the agreement between them is considered good. At $M_j$ = 0.7 (fig. 34(b)) inflow noise dominates the region between $\theta$ = 10° and 80°, and impact noise is dominant from 90° to at least 120°. This result agrees with the distribution of the velocity exponent $N$ shown in the lower portion of figure 34(b). At $M_j$ = 0.8 (fig. 34(c)) inflow noise ($U^6$ dependence) is dominant in the region between $\theta$ = 10° and 60°, and impact noise ($U^{9.5}$ dependence) is dominant at 100°. This result nominally agrees with the distribution of the velocity exponents shown in figure 34(c). The velocity dependence of impact noise is $U^8$ in figures 34(a) and (b) and $U^{9.5}$ in figure 34(c). The change in the velocity exponent with increased velocity results from the measured large-flat-board data of reference 20, upon which the impact noise is based. It is shown in reference 20 that the sound power had a velocity dependence of $U^8$ between $M_j$ = 0.4 and 0.7 and increased gradually at higher jet Mach numbers. Specifically, at $M_j$ = 0.8 the sound power had a velocity dependence of $U^{9.5}$.

Plugs in Slots

The OASPL distribution for the baseline configuration with plugs in the slots between the wing and flaps is presented in figure 35. The calculated estimate of trailing-edge noise (eq. (2)) is presented, along with the empirically based estimate of impact noise and the logarithmic sum of impact and trailing-edge noise ($OASPL_{impact, TE}$, eq. (5)). Inflow noise is not included because the plugs are assumed to minimize or substantially eliminate inflow about the flaps and wing.

At $M_j$ = 0.5 (fig. 35(a)), the logarithmic sum of impact noise and edge noise (eq. (5)) again is generally 1.5 decibels below the test data. Between 10° and 60° the curve representing equation (5) suggests the dominance of edge noise, which is sup-

ported by the distribution of the velocity exponent based on the measured data. Between $85^O$ and $115^O$ the dominance of impact noise is further supported by an increase in the velocity exponent N from 6.3 to 8.5.

At jet Mach numbers of 0.7 and 0.8 (figs. 35(b) and (c)) close agreement is shown between the measured data and the curve of $OASPL_{impact, TE}$. At $M_j = 0.7$, edge noise (eq. (2)) should be dominant between $\theta = 10^O$ and $40^O$, and impact noise from $80^O$ to $115^O$. The dominance of these two calculated noise sources is supported by the velocity exponents determined from the measured data and shown in figure 35(b). A similar comparison at $M_j = 0.8$ is also supported by agreement with the velocity exponents determined from measured data between $10^O$ and $115^O$.

A comparison between the spectral data of the baseline configuration and the baseline configuration with plugs (figs. 18 to 21 and 23 to 25) indicates that a reduction in noise in the frequency range between 250 and 315 hertz occurred with the addition of the plugs. This frequency range coincides with the frequencies of the first harmonic axisymmetric vortex mode of the large-scale turbulence structures in the jet flow field. This agreement implies that the large-scale turbulence structures inflowing about the wing and flaps may be related to the noise produced at 250 and 315 hertz.

Plugs and Slot Nozzle Blowing

The OASPL distributions for the baseline configuration with plugs and slot nozzle blowing are presented in figure 36. If it is assumed that the use of the plugs and slot nozzle blowing significantly reduces inflow and trailing-edge noise, respectively, then the only noise source remaining, according to the model presented in this report, is impact noise. Therefore, only the empirically based estimate of the impact noise is presented and compared with the measured data in figure 36.

A comparison of the measured data and impact noise at $M_j = 0.5$ (fig. 36(a)) shows clearly that the use of plugs and slot nozzle blowing did not reduce the noise generated to that predicted by impact noise only. However, the use of these suppression devices did reduce the noise approximately 2 decibels below the baseline configuration with plugs (compare figs. 35(a) and 36(a)). A nominal velocity exponent distribution of 5, presented in the lower portion of figure 36(a), also indicates that the noise generated was not impact noise, which has a $U^8$ velocity dependence.

At $M_j = 0.7$ and 0.8 (figs. 36(b) and (c), respectively) the measured data at $\theta = 40^O$ and $55^O$ have nominal velocity exponents of 6.0 and 5.7, respectively, which indicate that another noise source is present in addition to impact noise. At $\theta = 85^O$, however, fair agreement is shown between the level of the measured data and the predicted impact noise. This agreement is also supported by the velocity exponents determined

from the measured data and shown in figures 36(b) and (c).

These data indicate that the use of slot nozzle blowing is only partially effective in reducing trailing-edge noise. A more clear understanding of the effect of slot nozzle blowing can be obtained by referring to figures 20 and 21, which represent test data at $\theta = 40^{\circ}$ and $55^{\circ}$, respectively. When the spectra of the baseline configuration and the baseline configuration with plugs and slot nozzle blowing are compared, substantial noise reductions of 10 decibels in the low-frequency and midfrequency ranges are evident. These reductions may have extended into the higher frequency ranges if it were not for the noise produced by the slot nozzle itself, as discussed in the section EXPERIMENTAL RESULTS. Thus, it appears that trailing-edge blowing should produce substantial noise reductions in the frequency range between 250 hertz and 1.25 kilohertz with potential reductions at higher frequencies, provided the interaction noise produced by the slot nozzle flow field and the jet flow field passing over the trailing edge of the second flap can be diminished.

In summary, at jet Mach numbers of 0.5, 0.7, and 0.8, the use of the plugs and slot nozzle blowing was effective in suppressing inflow noise, partially effective in suppressing trailing-edge noise, and ineffective in suppressing impact noise. Thus, to reduce the noise beyond that obtained here, both trailing-edge noise and impact noise must be more effectively suppressed.


CONCLUDING REMARKS


Based on the results of these tests several implications may be noted. Because the large-scale turbulence structures of the jet appear to contribute to inflow noise and impact noise, inhibiting their production or growth should produce additional suppression. One way to inhibit the growth of these structures is to move the nozzle to within 2 nozzle diameters of the flaps. Although this arrangement would produce acoustic feedback, feedback can be suppressed by locating several small fingerlike rods in the nozzle exit flow field as suggested in reference 19. The advantages of moving the nozzle to within 2 nozzle diameters of the flaps are, first, exposure of the flaps to the smaller eddy sizes and pressure fluctuations present at this location in the nozzle core flow; second, improved noise suppression by devices applied to the flaps because of the exposure to the smaller eddy sizes; third, a significant reduction in the size of the large-scale turbulence structures of the jet flow field impacting the flaps; fourth, greater turning efficiency of the jet flow; fifth, reduction of the noise produced by inflow about the wing and first flap; and sixth, increased shielding by the flaps of the rearward quadrant beneath the engine and flaps from high-frequency noise.

Possible disadvantages include changes in the lift distribution over the wing-flap

19

combination, high surface temperatures resulting from a more focused and less diffused jet impingement on the flaps, and engine back pressure effects producing instability in the engine mass flow rate.


## SUMMARY OF RESULTS

The noise suppression effectiveness was determined for several devices applied separately and in combination to a large-scale model of the two-flap externally blown flap wing in its approach (baseline) configuration. The following results were obtained:

1. Use of an active blowing technique consisting of blowing secondary air through a slot nozzle located at the trailing edge of the second flap showed an average increase of 0.5 decibel above the noise produced by the baseline configuration. The additional noise was believed to be contributed by the slot nozzle.

2. Use of short spanwise plugs in the slots between the wing and flaps of the baseline configuration produced overall-sound-pressure-level noise reductions of 3 decibels in the forward quadrant below the nozzle and flaps in the flyover plane. This reduction occurred in the frequency range between 50 and 1000 hertz of the spectrum.

3. Combining the plugs and slot nozzle suppression devices produced up to a 4.5-decibel reduction of overall sound pressure level in the forward quadrant below the nozzle and flaps. A maximum noise reduction of 5 decibels occurred directly below the nozzle and flaps at a jet Mach number of 0.5 and decreased with increasing jet velocity. These noise reductions occurred between frequencies of 100 and 3150 hertz, with some reductions in sound pressure level of as much as 10 decibels. The spectra revealed two dominant sources of noise: The first was a strong low-frequency source with a peak between 100 and 125 hertz. This noise source dominated the forward quadrant below the nozzle and flaps. The second source had a peak between 250 and 400 hertz. This source was dominant directly below the nozzle and flaps.

4. Several existing noise source models were applied to the test results of the baseline configuration. These models included impact noise, produced by the jet exhaust impinging on the surface of the second flap; inflow noise, produced by the jet exhaust flow about the wing and flaps, which in turn produces a fluctuating lift response to an upwash disturbance; and trailing-edge noise, produced by the jet flow passing over the trailing edge of the second flap. The analysis indicates that the dominant noise directly beneath the nozzle, wing, and flaps is impact noise. The analytical relation compares favorably with measured data in magnitude and trend. Finally, the application of the analysis to the measured data shows that impact noise is not suppressed by trailing-edge blowing or the use of the plugs in the slots between the wing and flaps.

5. The frequency at which the peak sound pressure level of the baseline configuration occurred appears to be governed by the periodic formation and shedding of large-scale turbulence structures (ring vortices) from the outlet of the jet nozzle. This turbulence is believed to be the principal flow field structure which simultaneously is responsible for producing impact and inflow noise. These results suggest that additional noise suppression beyond that obtained with the suppression devices used here may result if the production or growth of these structures is inhibited.

Lewis Research Center,
    National Aeronautics and Space Administration,
        Cleveland, Ohio, January 28, 1976,
            505-03.

21

# APPENDIX A

## SYMBOLS

| | |
|---|---|
| $A$ | actual correlation area, $m^2$ |
| $A_c$ | ideal correlation area, $\pi l_1 l_2$, $m^2$ |
| $A_1, A_2, A_3$ | imaginary surface within which noise sources are located over flap surfaces |
| $a$ | effective radius of sound source, m |
| $b$ | span length, m |
| $C$ | chord length, m |
| $\left(C_L\right)_\alpha$ | steady-state effective lift coefficient slope, $deg^{-1}$ |
| $C_p$ | pressure coefficient, $(P_1 - P_{atm})/(\rho_m U_m^2/2)$ |
| $c$ | speed of sound, m/sec |
| $D$ | nozzle exit diameter, m |
| $F'_L$ | fluctuating lift force, N |
| $f$ | frequency, Hz |
| $\Delta f$ | one-third-octave band width, Hz |
| $f_c$ | cutoff frequency, Hz |
| $f_r$ | characteristic frequency of fluctuating lift forces, Hz |
| $k$ | acoustic wave number, $\omega/c$, $m^{-1}$ |
| $L$ | source dimension, m |
| $L'$ | ratio of turbulence integral scale length to airfoil semichord |
| $l_1$ | streamwise semiaxial length of ellipse, m |
| $l_2$ | spanwise semiaxial length of ellipse, m |
| $M_j$ | jet exit Mach number |
| $M_l$ | local Mach number evaluated on jet axis |
| $N$ | magnitude of velocity exponent |
| OASPL | overall sound pressure level |
| $P$ | pressure, $N/m^2$ |

$\overline{P^2}$          mean square sound pressure, $N^2/m^4$

$P_{ref}$        reference sound pressure, 20 $\mu N/m^2$

$r$             distance between observer and trailing edge, m

SPL        sound pressure level

$U$           mean flow velocity, m/sec

$U_c$         eddy convection speed, m/sec

$U_l$         local mean flow velocity evaluated on jet axis, m/sec

$U_m$       maximum mean velocity of free shear layer at trailing edge of flap, m/sec

$v'$           turbulence velocity fluctuation normal to airfoil chord and leading edge, m/sec

$W$         one-half of spanwise width of velocity profile between points where local velocity is equal to $U_m/2$ at trailing edge of flap, m

$x, y, z, z'$    Cartesian coordinates (figs. 6 and 11)

$\beta$           angle between fluctuating force vector and observer (fig. 37), deg

$\delta$           thickness of boundary layer, m

$\delta_e$         characteristic eddy scale length, $2\pi l_1$, m

$\theta$           radiation angle measured from nozzle inlet axis (figs. 5 and 37), deg

$\rho$           density of undisturbed fluid, $kg/m^3$

$\rho_l$         density of fluid evaluated at point where $U_l$ is determined, $kg/m^3$

$\sum SPL$    sound pressure level (antilogarithmic) over a specified frequency range, dB re 20 $\mu N/m^2$

$\varphi_F$        force spectral density, N/Hz

$\varphi_P$        sound pressure spectral density, $N/(m^2)(Hz)$

$\psi$           angle defined in fig. 11, deg

$\omega$          radian frequency, $sec^{-1}$

Subscripts:

atm        atmospheric

exp         exponential

i             impingement

| | |
|---|---|
| impact | impact |
| impinge | impingement |
| inflow | inflow |
| j | jet exit condition |
| L | lower |
| $l$ | local |
| slot | slot |
| TE | trailing edge |
| u | upper |
| 1 | point 1 |
| 2 | point 2 |

# APPENDIX B

## DERIVATION OF EQUATIONS FOR INFLOW NOISE

Reference 4 implies that the dominant noise beneath the UTW EBF STOL aircraft results when the jet impacts the flap and/or unsteady inflow occurs near the leading edge of the flaps. Also it is suggested that this noise is related to the observed large-scale turbulence structures or ring vortices present in jet flow which were studied extensively in the work of reference 19 and discussed in reference 4. In particular, it is speculated in reference 4 that these turbulence structures produce unsteady inflow about the flaps causing fluctuating lift, which may produce noise. The shedding frequency of these structures from the nozzle lip is shown in reference 19 to be related to the frequency at which the far field peak sound pressure level occurred for several jet impingement experiments at different Mach numbers.

Reference 17 presents an estimate of the noise for cases in which the source is considered intermediate between satisfying the conditions for compactness (kL $\ll$ 1) and noncompactness (kL $\gg$ 1, where k is the acoustic wave number $\omega/c$ and L is the source dimension). According to reference 25 the overall power radiated as a result of fluctuating lift is independent of the orientation of a surface to the mean flow passing over it if the dimensions of the reflecting surface are comparable with or greater than one-quarter of the acoustic wavelength. It is also emphasized, however, that the distribution in angle of the radiated intensity does depend on the orientation of the surface. In the following derivation these conditions are assumed to be satisfied. The derivation presents an estimate of the OASPL noise from inflow of the large-scale turbulence structures about the wing and flaps of the UTW EBF in its approach configuration. The inflow turbulence spectrum used in the derivation is assumed to consist of a unique size eddy referred to in this report as the large-scale turbulence structure of the jet flow.

A rigid airfoil of chord C and span b immersed in a subsonic turbulent inflow is analyzed in reference 17. For the case where the ratio of the characteristic eddy size to the chord length is not small, an application of some form of quasi-steady solution is suggested to describe the lift fluctuations. Once the lift fluctuations are described, the surface is modeled as a small (i.e., small with respect to a wavelength) spherical source, and the point dipole expression is modified to account for reduced radiation at ratios of acoustic wavelength to body size which are small with respect to the chord.

The far field sound pressure spectral density $\varphi_p$ of an arbitrarily oriented finite source is represented by equation (13) of reference 17. The following form of equation (13) expresses the sound pressure spectral density distribution as a function of the force spectral density $\varphi_F$ in a plane perpendicular to the airfoil chord line and leading edge:

$$\varphi_{\mathbf{P}}(r, \beta, \omega) = \frac{\varphi_{\mathbf{F}}(\omega)}{16\pi^2 r^2} \left( \frac{k^2}{1 + a^2 k^2} \right) \cos^2 \beta \tag{B1}$$

The original symbols are changed to the present nomenclature (see fig. 37 for the co-ordinate system). From the relation given by

$$\frac{\varphi_{\mathbf{P}}(r, \beta, \omega)}{\varphi_{\mathbf{F}}(\omega)} = \frac{\overline{P^2}(r, \beta, \omega)}{\left[ F'_{\mathbf{L}}(\omega) \right]^2}$$

equation (B1) may be rewritten in the form

$$\overline{P^2}(r, \beta, \omega) = \frac{\left[ F'_{\mathbf{L}}(\omega) \right]^2}{16\pi^2 r^2} \left( \frac{k^2}{1 + a^2 k^2} \right) \cos^2 \beta \tag{B2}$$

From reference 17, for a two-dimensional airfoil passing through a single large-scale two-dimensional eddy, the fluctuating lift force $F'_{\mathbf{L}}(\omega)$ is approximated by

$$F'_{\mathbf{L}} \approx \left( C_{\mathbf{L}} \right)_\alpha \frac{1}{2} \rho_l (U_l)^2 A_c \frac{v'}{U_l} \tag{B3}$$

where the original symbols are changed to the present nomenclature. In equation (B3), $A_c$ is the ideal correlation area, which from reference 25 is of the order of the area $\pi l_1 l_2$, an ellipse having a streamwise semiaxial length $l_1$ and a spanwise semiaxial length $l_2$, and $v'/U_l$ is the upwash turbulence intensity in the direction normal to both the airfoil chord and leading edge (ref. 25). Reference 17 notes $\left( C_{\mathbf{L}} \right)_\alpha$ is the transfer function between the upwash disturbance $v'$ and the lift response of the airfoil. Substituting equation (B3) into equation (B2) and rearranging yield

$$\overline{P^2}(r, \beta, \omega) = \left[ (C_{\mathbf{L}})_\alpha \frac{\left( \dfrac{\rho_l U_l^2}{2} \right) \left( \dfrac{v'}{U_l} \right) \cos \beta \sqrt{A_c}}{4\pi r} \right]^2 \left( \frac{A_c k^2}{1 + a^2 k^2} \right) \tag{B4}$$

26

It is indicated in reference 25 that the characteristic frequency of the fluctuating lift force is directly proportional to the eddy convection speed $U_c$ and inversely proportional to the characteristic eddy scale length $\delta_e$ (typical "wavelength" of eddy). Therefore,

$$f_r = \frac{U_c}{\delta_e} \tag{B5}$$

where $\delta_e$ is of the order of $2\pi l_1$ and $l_1$ is of the order of $3l_2$. In reference 19 the convection speed of the large-scale turbulence structures is indicated to be 0.63 of the local jet velocity $U_l$. Therefore, substituting for $\delta_e$ and $U_c$ in equation (B5) yields

$$f_r = \frac{0.63\, U_l}{6\pi l_2} \tag{B6}$$

A further simplification of equation (B4) occurs by considering the last term of equation (B4),

$$\frac{A_c k^2}{1 + a^2 k^2} \tag{B7}$$

where from reference 25

$$A_c = \pi l_1 l_2$$

Substituting for $l_1$ in terms of $l_2$ yields

$$A_c = 3\pi l_2^2 \tag{B8}$$

The area $A_c$ may also be expressed by letting

$$A_c = \pi a^2 \tag{B9}$$

where $a$ is the effective radius of $A_c$. If equations (B8) and (B9) are equated, the effective radius $a$ may be expressed as

$$a = \sqrt{3}\, l_2 \tag{B10}$$

Substituting $f_r$ from equation (B6) into the expression for the acoustic wave number $k$ and simplifying yield

$$k = \frac{0.21\, M_l}{l_2} \tag{B11}$$

Finally, substituting equations (B8), (B10), and (B11) into (B7) and simplifying result in

$$\frac{A_c k^2}{1 + a^2 k^2} = \frac{\pi}{\dfrac{7.559}{M_l^2} + 1} \tag{B12}$$

Substituting equation (B12) into equation (B4) and simplifying gives the mean square sound pressure in the form

$$\overline{P^2}(r, \beta, \omega) = \left[ \frac{(C_L)_\alpha \rho_l U_l^2 \left(\dfrac{v'}{U_l}\right)}{8\pi r} \right]^2 A_c \left( \frac{\pi}{\dfrac{7.559}{M_l^2} + 1} \right) \cos^2 \beta \tag{B13}$$

An expression for the effective lift coefficient slope $(C_L)_\alpha$ in equation (B13) is presented in reference 26. The coefficient $(C_L)_\alpha$ is a function of $L'$, where $L'$ is the ratio of the turbulence integral scale length $l_1$ to the airfoil semichord $C/2$, and is derived for an infinitesimal spanwise strip. The expression is based on the assumption of an infinite span airfoil encountering an arbitrary two-dimensional upwash field. The following is an approximate form (for $L' \leq 3$) of the expression from reference 26 which gives the mean square of the effective lift coefficient slope:

$$\overline{(C_L)_\alpha^2} \approx 2\pi^2 \frac{\ln\left[1.2 + \dfrac{\pi^2}{(L')^2}\right]}{\ln 1.2 + 3\dfrac{\pi^2}{(L')^2}} \tag{B14}$$

28

The turbulence intensity $v'/U_l$ of the large-scale turbulence structures was investigated in the study of reference 27. The same type of turbulence-shear interaction source terms was concluded to exist in the spectrum for the large-scale eddies as for the smaller ones. Therefore, the turbulence intensity in equation (B13) is assumed to be a function of the small eddy turbulence intensities.

The sound pressure level SPL determined as a function of the characteristic frequency $f_r$ of the fluctuating lift forces is given by

$$SPL(f_r) = 10 \log \frac{P^2}{P^2_{ref}} \tag{B15}$$

where from equation (B6) the characteristic frequency $f_r$ is evaluated from $f_r = 0.105 \, U_l / \pi l_2$ and $P_{ref} = 2 \times 10^{-5}$ newton per square meter. Because the turbulence spectrum used in this derivation is assumed to be composed of a unique eddy, the sound pressure level, based on a one-third-octave bandwidth, is given by

$$SPL_{1/3 \text{ band}} = SPL(f_r) + 10 \log \Delta f \tag{B16}$$

where $\Delta f = (f_c)_u - (f_c)_L$. The ratio of the upper cutoff frequency $(f_c)_u$ to the lower cutoff frequency $(f_c)_L$ for a one-third-octave bandwidth from reference 28 is given by

$$\frac{(f_c)_u}{(f_c)_L} = \sqrt[3]{2}$$

Because the center frequency is given by

$$f_r = \frac{(f_c)_u + (f_c)_L}{2}$$

$\Delta f$ may be expressed, after manipulation, as

$$\Delta f = 0.23 \, f_r \tag{B17}$$

Because the one-third-octave SPL produced by a unique type of eddy is assumed approximated by equation (B16), the overall sound pressure level produced by that same eddy is given by letting

$$OASPL_{inflow} = SPL_{1/3 \text{ band}} \tag{B18}$$

29

Finally, the expression for the one-third-octave inflow noise produced by a two-dimensional airfoil passing through a flow field having a turbulence spectrum consisting of a single large-scale turbulent eddy is obtained by substituting equations (B13), (B15), (B16), and (B17) into equation (B18):

$$\text{OASPL}_{\text{inflow}} = 10 \log \left[ \frac{\left( C_{\text{L}} \right)_{\alpha} \rho_{l} U_{l}^{2}}{r} \right]^{2} + 10 \log A_{\text{c}} + 10 \log \frac{\pi}{\frac{7.559}{M_{l}^{2}} + 1}$$

$$+ 10 \log \left( \frac{\frac{v'}{U_{l}}}{8\pi P_{\text{ref}}} \right)^{2} + 10 \log \cos^{2}\beta + 10 \log 0.23 \, f_{\text{r}} \quad \text{(B19)}$$

In order to apply equation (B19) to the UTW EBF baseline configuration considered in this report, it is necessary to adjust the idealized correlation area $A_{\text{c}}$ (eq. (B8)) to the actual correlation area A. This is done by multiplying $A_{\text{c}}$ in equation (B19) by $A/A_{\text{c}}$. Thus, equation (B19) may be expressed in the form

$$\text{OASPL}_{\text{inflow}} = 10 \log \left[ \frac{\left( C_{\text{L}} \right)_{\alpha} \rho_{l} U_{l}^{2}}{r} \right]^{2} + 10 \log \left( A \frac{A}{A_{\text{c}}} \right) + 10 \log \left[ \frac{A}{A_{\text{c}}} \left( \frac{\pi}{\frac{7.559}{M_{l}^{2}} + 1} \right) \right]$$

$$+ 10 \log \left( \frac{\frac{v'}{U_{l}}}{8\pi P_{\text{ref}}} \right)^{2} + 10 \log \cos^{2}\beta + 10 \log (0.23 \, f_{\text{r}}) \quad \text{(3)}$$

The correlation area A is estimated by considering the flow field in contact with the wing and each of the flaps. It is assumed in this analysis that small eddies, which constitute the main portion of the jet mixing region, in the vicinity of these airfoils produce surface pressure fluctuations that tend to cancel everywhere except at the airfoil

trailing edge; thus, these eddies produce trailing-edge noise. They also produce boundary-layer or surface scrubbing noise, which is assumed to be negligible in comparison with impact, inflow, or edge noise. The other eddies in the flow field consist of the large-scale turbulence structures which are convected along with the jet flow field (ref. 19). Because these eddies are larger than the chord lengths of either of the flaps at the downstream locations of the flaps, they will inflow about the flaps and produce inflow noise. Also, the peripheries of these eddies graze the lower surface of the wing, which may produce inflow about the wing. Therefore, it is assumed in this analysis that these large-scale turbulence eddies inflow about the first and second flaps and by grazing the wing induce inflow about the wing.

The actual correlation area $A$, like the ideal correlation area $A_c$, is assumed to be a function of the size of the large-scale turbulence structures. Reference 18 indicates that the loads on an airfoil which are induced by these structures are concentrated near them with the maximum to the side of their plane of symmetry. Reference 29 determined the actual correlation area $A$ from the pressure distribution over the surface of a circular flat plate impacted by a jet. The technique involved fitting a parabolic curve to the plate surface pressure distribution and determining the spanwise length at which the curve breaks away from the pressure distribution. This length was used in calculating the correlation area.

The technique of reference 29 was applied to the flaps of the baseline configuration. This was done by assuming that the pressure distribution over the lower or impact surface of each flap was approximated by the jet velocity profile of a freely expanding jet at stations downstream from the nozzle exit plane corresponding to the location of the midchord of the flaps. The spanwise lengths determined in this way for the first and second flaps were estimated to be one-quarter of the diameter of the freely expanding jet or equivalently $l_2/2$. These lengths multiplied by the individual flap chord lengths determined the correlation areas for the flaps. The use of the chord as the streamwise dimension of the correlation area is based on the assumption that, as the large-scale turbulence structures traverse each flap, their scale length remains effectively constant over the flap chord length.

The technique of reference 29 was applied to the wing by using the data of reference 30. Figure 14 of reference 30 presents a plot of isobar contours for jet flow grazing a flat plate oriented in a similar way to a nozzle as the wing to the nozzle of the baseline configuration discussed in this report. The spanwise length of the correlation area $A$ determined for the wing was estimated to be 0.8 of the nozzle exit diameter. This length multiplied by that portion of the wing chord length between the location of the zero isobar on the lower surface of the wing and the wing trailing edge determined the wing correlation area.

The gas properties $\rho_l$, $U_l$, and $M_l$ were determined on the jet axis at streamwise stations corresponding to the location of the midchord of each flap and the midpoint of

the wing correlation length. The magnitudes of $U_l$ were determined from the jet velocity decay relations of reference 24 for a single nozzle.

The upwash turbulence intensity $v'/U_l$ was determined from plots of radial and axial free jet turbulence intensities presented in figures 16 and 19 of reference 31. These axial and radial intensities were graphically related to provide the component perpendicular to the chord line of the wing and flaps. The values were determined for the wing and flaps at the same streamwise axial stations as the gas properties, but at radial locations off the jet axis corresponding to the midchord on the impact or lower surfaces of the wing and flaps. Thus, the upwash turbulence intensities, like the gas properties, represent averaged values over the chordwise lengths of the wing and flaps. The values of the upwash turbulence intensities determined for the wing, first flap, and second flap were 0.025, 0.077, and 0.160, respectively.

The angle $\beta$ of equation (3) is shown schematically in figure 37 as the angle between the resultant fluctuating lift force $F'_L$, which is perpendicular to the chord line of an airfoil, and the observer in the far field. In the tests discussed in this report $\beta$ was determined graphically as a function of the acoustic radiation angle $\theta$ for the wing and each of the flaps. However, $\beta$ can be crudely approximately for the wing, first flap, and second flap by being set equal to $\theta - 85^{\circ}$, $\theta - 55^{\circ}$, and $\theta - 25^{\circ}$, respectively.

## REFERENCES

1. Maglieri, Dominic J.; and Hubbard, Harvey H.: Preliminary Measurements of the Noise Characteristics of Some Jet-Augmented-Flap Configurations. NASA MEMO 12-4-58L, 1959.

2. Dorsch, R. G.; Krejsa, E. A.; and Olsen, W. A.: Blown Flap Noise Research. AIAA Paper 71-745, June. 1971.

3. Dorsch, R. C.: Externally Blown Flap Noise Research. SAE Paper 740468, Apr-May 1974.

4. McKinzie, Daniel J., Jr.; and Burns, Robert J.: Analysis of Noise Produced by Jet Impingement Near the Trailing Edge of a Flat and a Curved Plate. NASA TM X-3171, 1975.

5. Pinkel, Benjamin; and Scharton, Terry D.: Reduction of Noise Generated by Flow of Fluid Over a Plate. Acoust. Soc. Am. J., vol. 53, no. 4, Apr. 1973, pp. 1184-1185.

6. Sharton, Terry D.; Pinkel, Benjamin; and Wilby, John F.: A Study of Trailing Edge Blowing as a Means of Reducing Noise Generated by the Interaction of Flow with a Surface. (BBN-2593 Bolt, Beranek and Newman, Inc., NAS1-9559) NASA CR-132270, 1973.

7. McKinzie, D. J., Jr.; and Burns, R. J.: Externally Blown Flap Trailing Edge Noise Reduction by Slot Blowing - A Preliminary Study. AIAA Paper 73-245, Jan. 1973.

8. Hayden, Richard E.; Kadman, Yoram; and Chanaud, Robert C.: A Study of the Variable Impedance Surface Concept as a Means for Reducing Noise from Jet Interaction with Developed Lift-Augmenting Flaps. (BBN-2399, Bolt, Beranek, and Newman, Inc.; NAS1-9559), NASA CR-112166, 1972.

9. Pennock, A. P.; Swift, G.; and Marbert, J. A.: Static and Wind Tunnel Model Tests for the Development of Externally Blown Flap Noise Reduction Techniques. (LG74ER0170, Lockheed-Georgia Co.; NAS3-16831) NASA CR-134675, 1975.

10. Burns, Robert J.; and McKinzie, Daniel J., Jr.; and Wagner, Jack M.: Effects of Perforated Flap Surfaces and Screens on Acoustics of a Large Externally Blown Flap Model. NASA TM X-3335, 1976.

11. Olsen, William A.; Dorsch, Robert G.; and Milles, Jeffrey H.: Noise Produced by a Small-Scale Externally Blown Flap. NASA TN D-6636, 1972.

12. Howes, Walton L.: Ground Reflection of Jet Noise. NASA TR R-35, 1959.

13. Standard Values of Atmospheric Absorption as a Function of Temperature and Humidity for Use in Evaluating Aircraft Flyover Noise. Aerospace Recommended Practice 866, SAE, Aug. 1964.

14. Fink, M. R.: Mechanisms of Externally Blown Flap Noise. AIAA Paper 73-1029, Oct. 1973.

15. Guinn, Willy A.; Blankey, Dennis F.; and Gibson, John S.: V/STOL Noise Prediction and Reduction. LG73ER0062, Lockheed-Georgia Co. (FAA-RD-73-145), 1973.

16. Ffowcs Williams, J. E.; and Hall, L. H.: Aerodynamic Sound Generation by Turbulent Flow in the Vicinity of a Scattering Half Plane. J. Fluid Mech., vol. 40, pt. 4, Mar. 1970, pp. 657-670.

17. Hayden, Richard E.: Noise from Interaction of Flow with Rigid Surfaces: A Review of Current Status of Prediction Techniques. NASA CR-2126, 1972.

18. Fink, M. R.: Experimental Evaluation of Trailing Edge and Incidence Fluctuation Noise Theories. AIAA Paper 75-206, Jan. 1975.

19. Neuwerth, Günther: Acoustic Feedback Phenomena of the Subsonic and Hypersonic Free Jet Impinging on a Foreign Body. NASA TT F-15719, 1974.

20. Olsen, William A.; Miles, Jeffrey H.; and Dorsch, Robert G.: Noise Generated by Impingement of a Jet Upon a Large Flat Board. NASA TN D-7075, 1972.

21. Dorsch, R. G.; Kreim, W. J.; and Olsen, W. A.: Externally Blown-Flap Noise. AIAA Paper 72-129, Jan. 1972.

22. Johnson, William G., Jr.: Longitudinal Aerodynamic Characteristics of a Wing-Body Configuration Having a Rectangular Aspect Height and Ratio 6, Slotted Super Critical Wing with Externally Blown Flaps. NASA TM X-2388, 1971.

23. von Glahn, U. H.; Groesbeck, D.; and Reshotko, M.: Geometry Considerations for Jet Noise Shielding with CTOL Engine-Over-The-Wing Concept. NASA TM X-71562, 1974.

24. von Glahn, U. H.; Groesbeck, D. E.; and Huff, R. G.: Peak Axial-Velocity Decay with Single- and Multi-Element Nozzles. NASA TM X-67979, 1972.

25. Sharland, I. J.: Sources of Noise in Axial Flow Fans. J. Sound Vibration, vol. 1, no. 3, Mar. 1964, pp. 302-322.

26. Filotas, L. T.: Theory of Airfoil Response in a Gusty Atmosphere. Part 2: Response to Discrete Gusts of Continuous Turbulence. UTIAS-141, Toronto Univ. (AD-700774; AFOSR-69-3089TR), 1969.

27. Arndt, Roger E. Q.; and George, W. K.: Investigation of the Large-Scale Coherent Structure in a Jet and Its Relevance to Jet Noise. (Penn. State Univ.; NGR-39-009-270) NASA CR-138908, 1974.

28. Beranek, Leo L., ed.: Noise Reduction. McGraw-Hill Book Co., Inc., 1960, p. 73.

29. Siddon, Thomas E.: Surface Dipole Strength by Cross-Correlation Method. Acoust. Soc. Am. J., vol. 53, no. 2, 1973, pp. 619-633.

30. Foss, John F.; and Kleis, Stanley, J.: The Oblique Impingement of an Axisymmetric Jet. (Michigan State Univ.; NASA Grant NGR 23-004-068.) NASA CR-134961, 1976.

31. Donaldson, Coleman Dup.; Snedeker, Richard S.; and Margolis, David P.: A Study of Free Jet Impingement. Part 2. Free Jet Turbulence Structure and Impingement Heat Transfer. J. Fluid Mech., vol. 45, pt. 3, Feb. 1971, pp. 477-512.
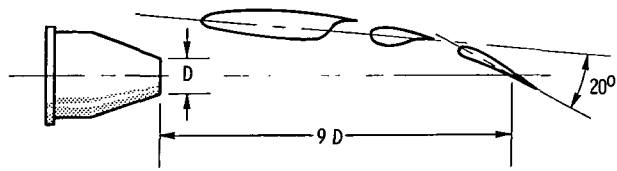
(a) Takeoff configuration.
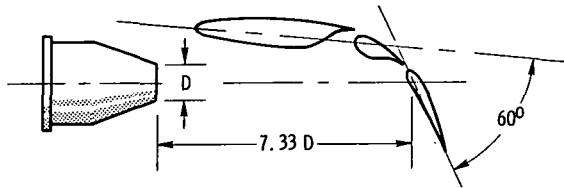


(b) Approach configuration.

Figure 1. – Takeoff and approach configurations for externally blown flap with conical nozzle.
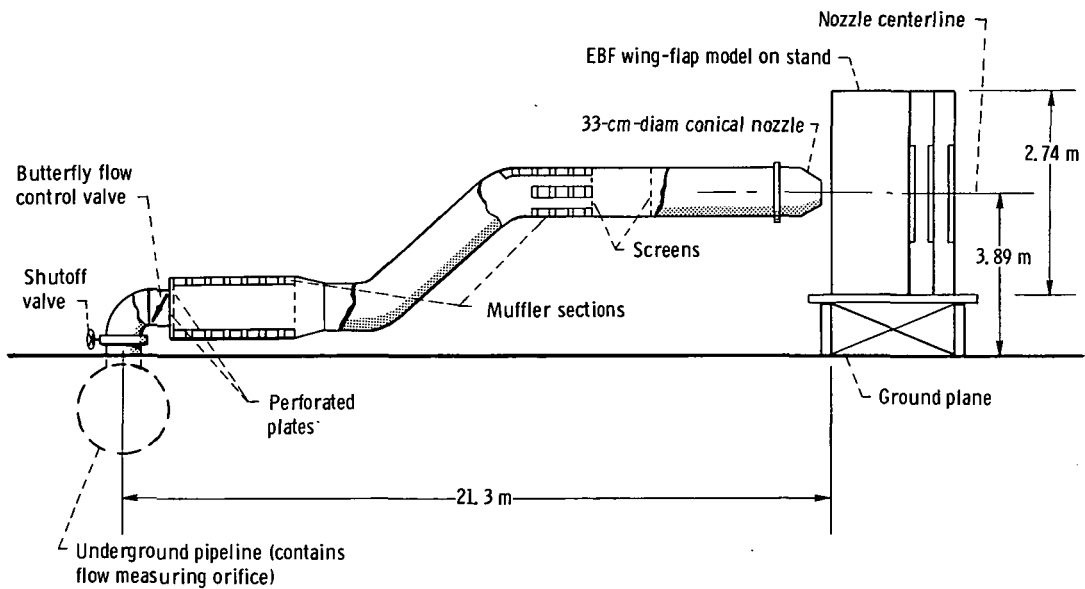


Figure 2. – Diagram of externally blown flap large-scale test facility showing primary airflow system.
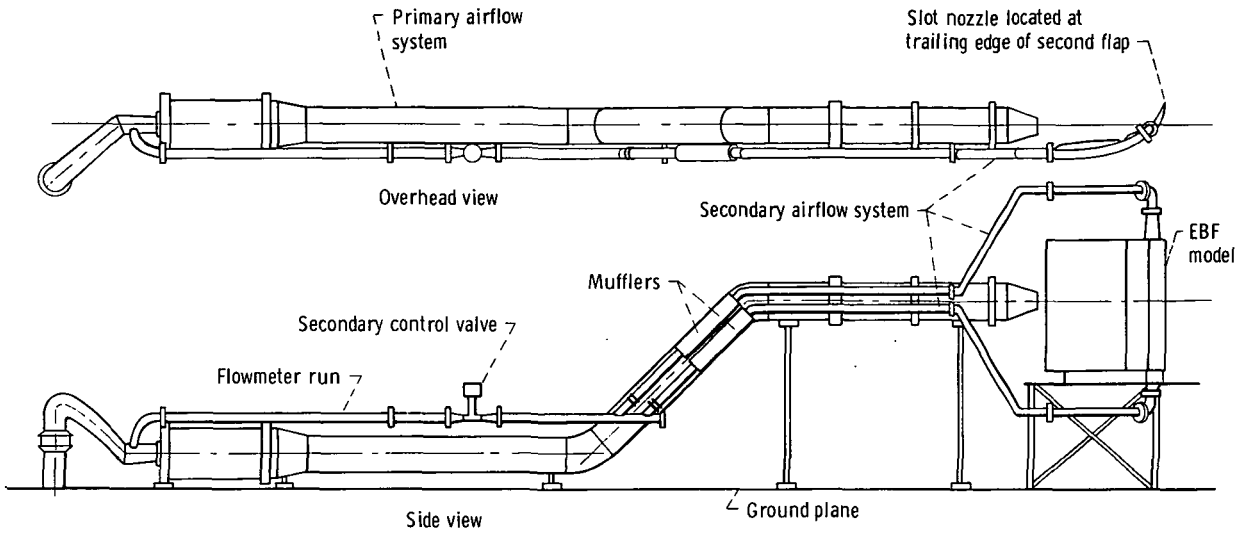
Figure 3. – Diagrams of externally blown flap test facility showing secondary airflow system to slot nozzle on trailing edge of second flap.



| Tap | Distance between tap and next tap, cm |
|-----|----------------|
| 1 | ---- |
| 2 | 2.54 |
| 3 | 5.08 |
| 4 | 6.6 |
| 5 | 8.6 |
| 6 | 7.6 |
| 7 | 7.6 |
| 8 | 7.6 |
| 9 | 7.6 |
| 10 | 4.6 |
| 11 | ---- |
| 12 | 6.35 |
| 13 | 7.6 |
| 14 | 7.6 |
| 15 | 7.6 |
| 16 | 7.6 |
| 17 | 5.1 |
| 18 | 5.1 |
| 19 | 5.1 |
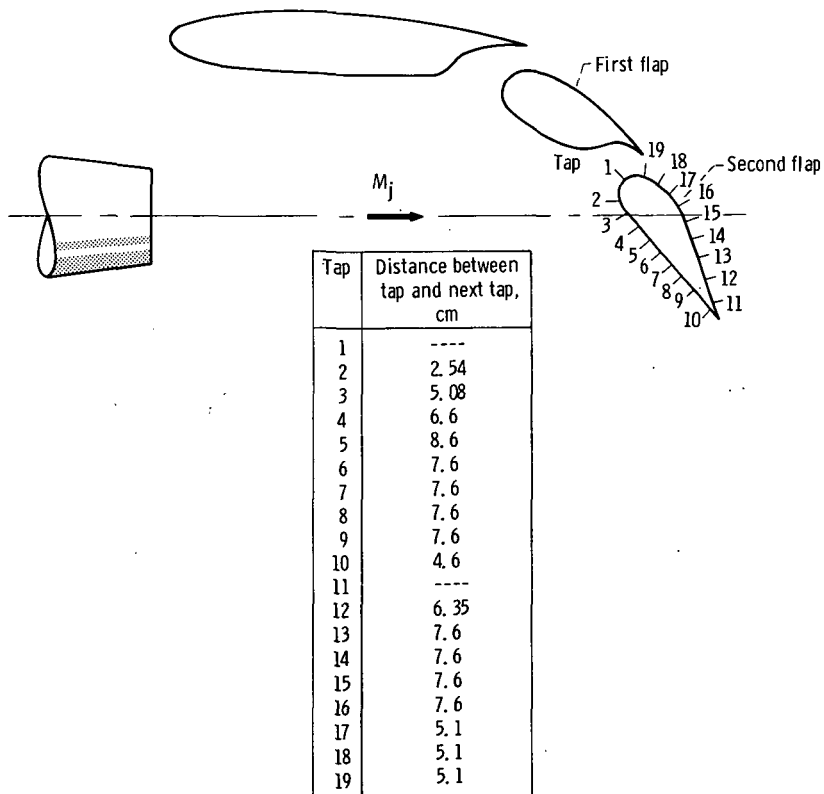
Figure 4. – Static-pressure-tap locations over surface of second flap.
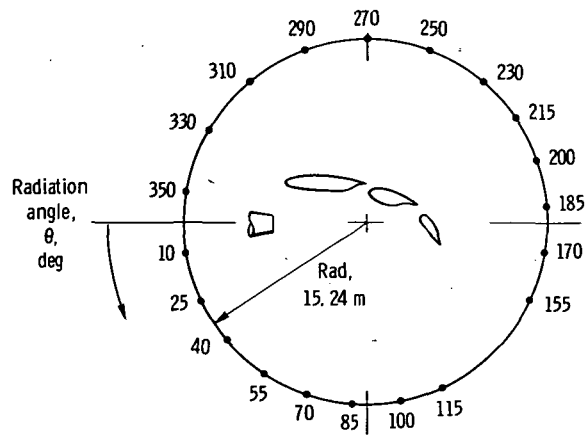
Figure 5. - Microphone circle locations relative to wing flaps.
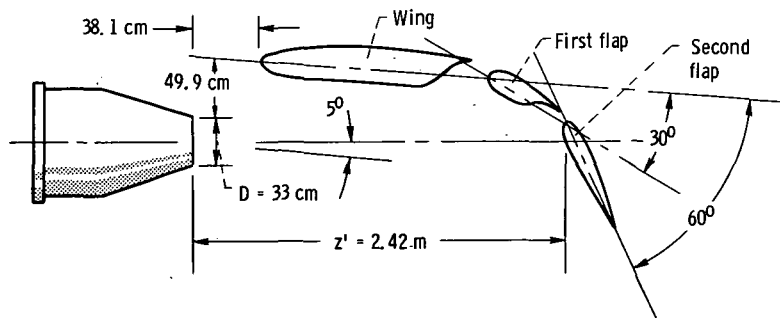


Figure 6. - Location of conical nozzle relative to wing-flap landing configuration.
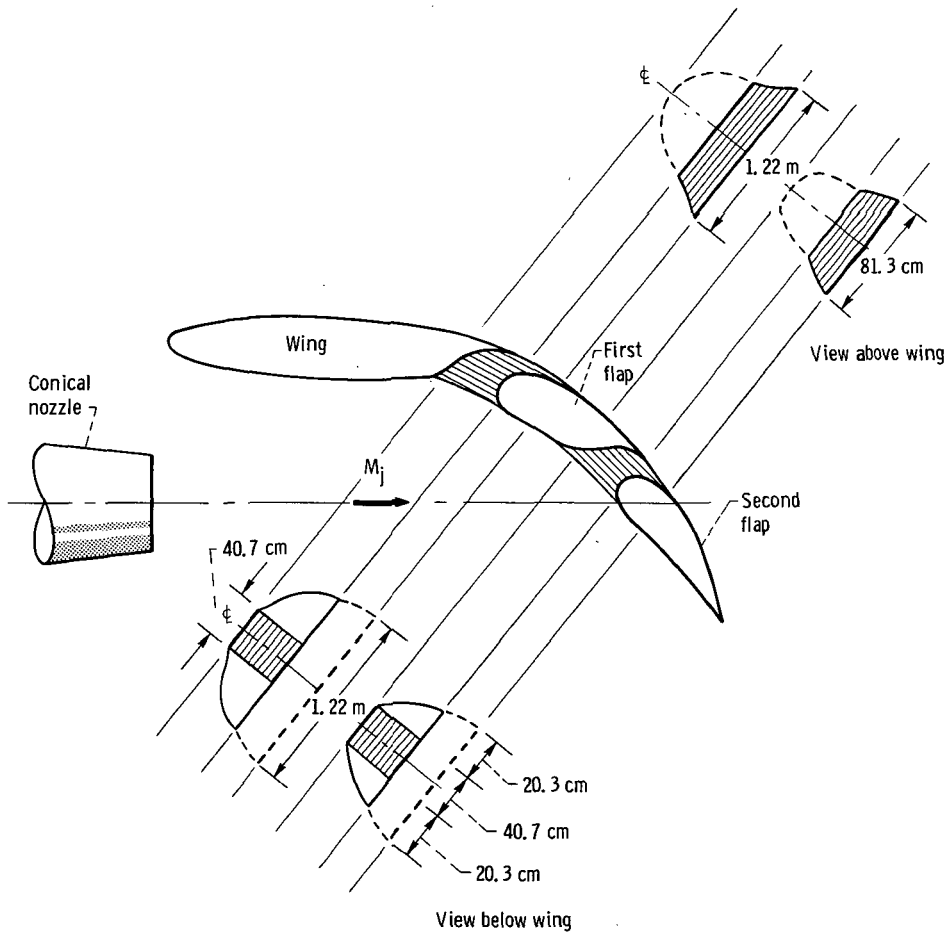
Figure 7. - Plug fairings in slots between wing and first flap and first and second flaps.

Slot
blocked
off

Plenum chamber
and two orifice
plates

1. 22 m

2. 74 m

Open
slot

Slot
blocked
off

CD-11953-02
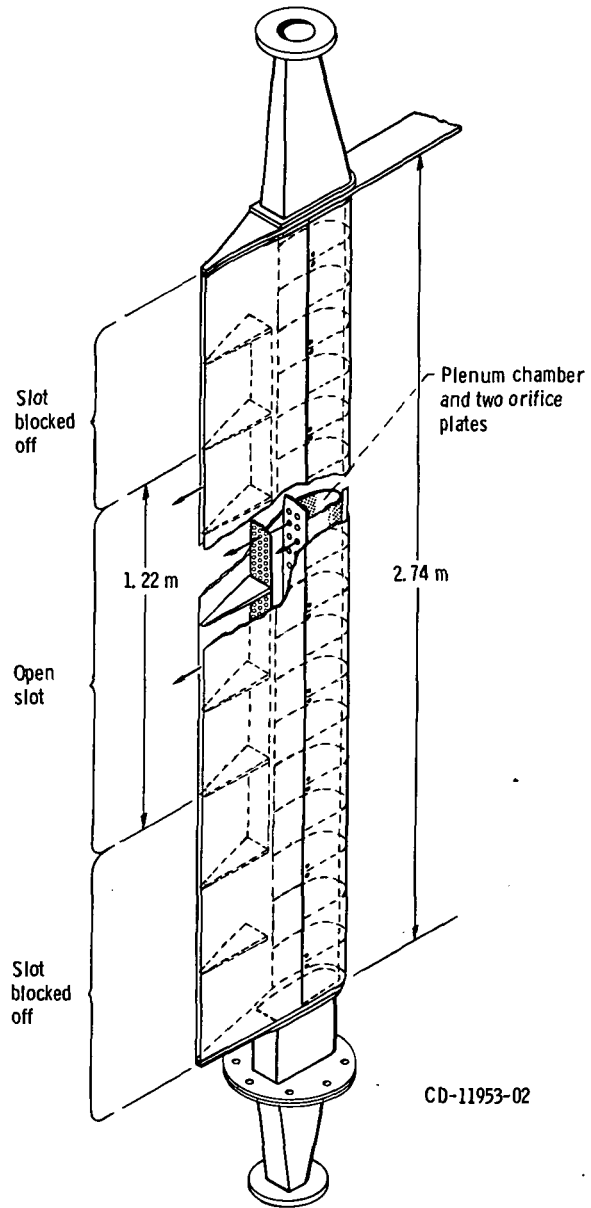
Figure 8. - Diagram of second flap showing slot nozzle and plenum chamber.
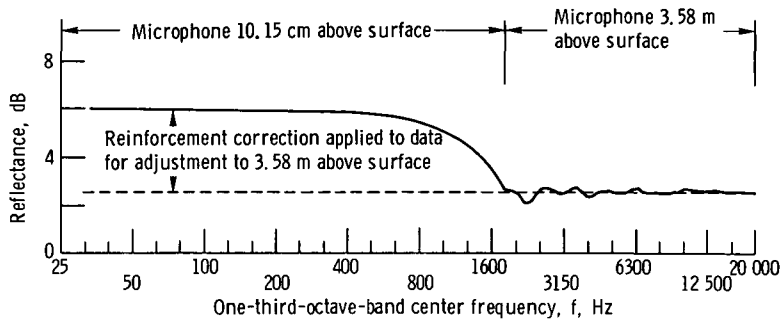
Figure 9. – Combined reflectance correction to microphone data taken 10.15 centimeters and 3.58 meters above ideal reflecting surface.



(a) Noise regions.



(b) Noise sources.
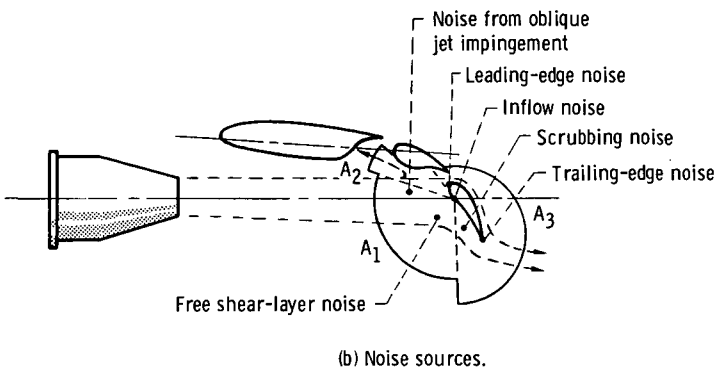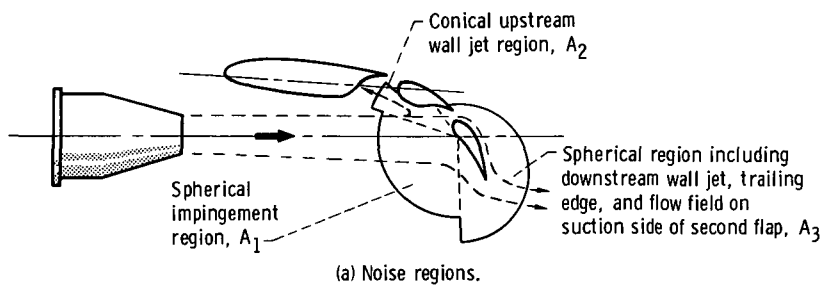
Figure 10. – Jet impinging on externally blown flap two-flap wing in its approach configuration.

41
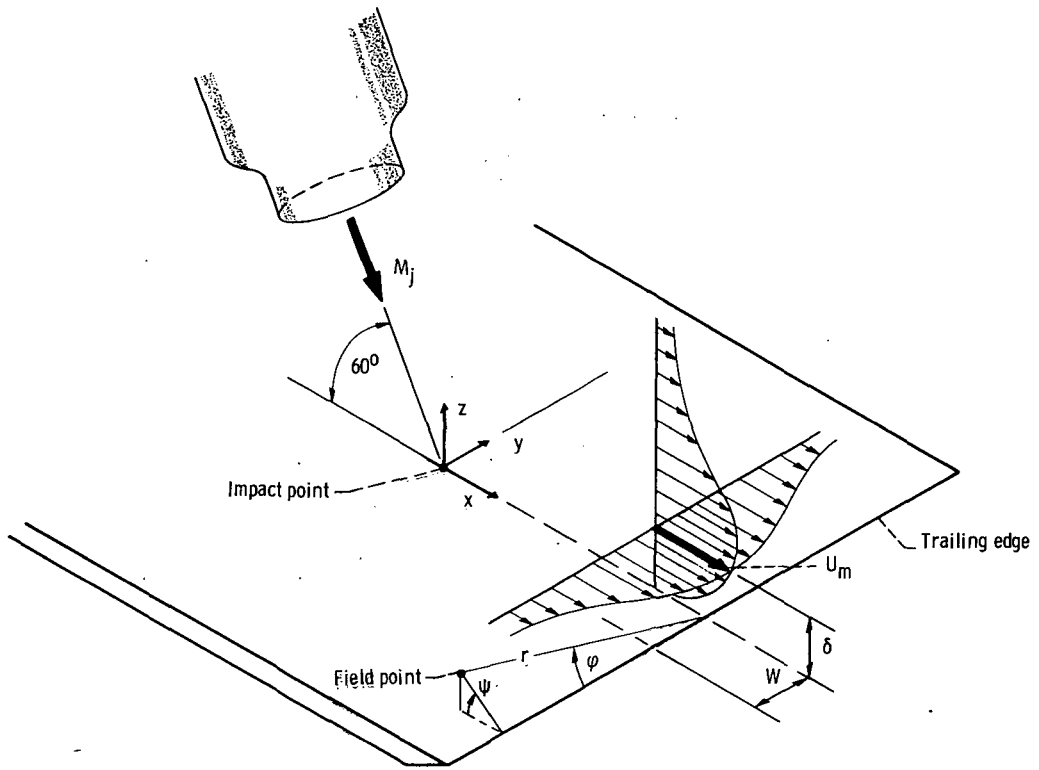
Figure 11. – Coordinate system of jet impinging on semi-infinite half-plane near its trailing edge (from ref. 4).
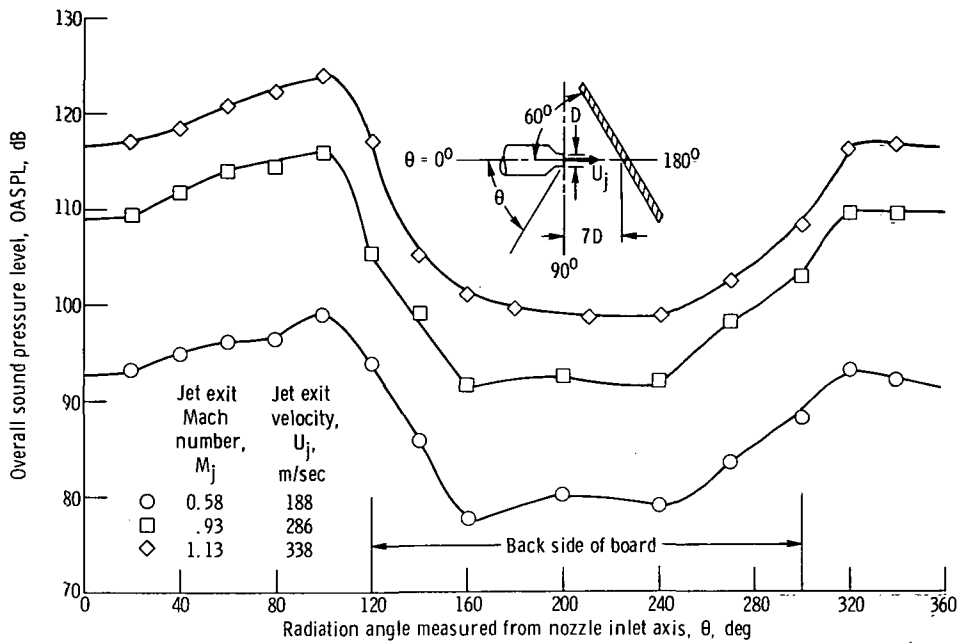
Figure 12. - Overall-sound-pressure-level distribution for large flat board. Nozzle exit diameter D, 5.2 centimeters; azimuthal angle, $0^0$ (from ref. 20).



Figure 13. - Overall-sound-pressure-level distribution for two-flap externally blown flap baseline configuration with $30^0$ to $60^0$ flaps (approach configuration).

Figure 14. - Sound-pressure-level spectra for two-flap externally blown flap baseline configuration with 30° to 60° flaps (approach configuration).
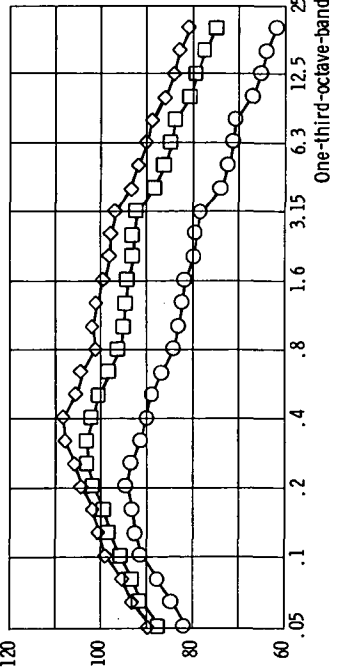
44

Figure 14. – Continued.

(m) Radiation angle measured from nozzle inlet axis θ, 230°.

(n) Radiation angle measured from nozzle inlet axis θ, 250°.

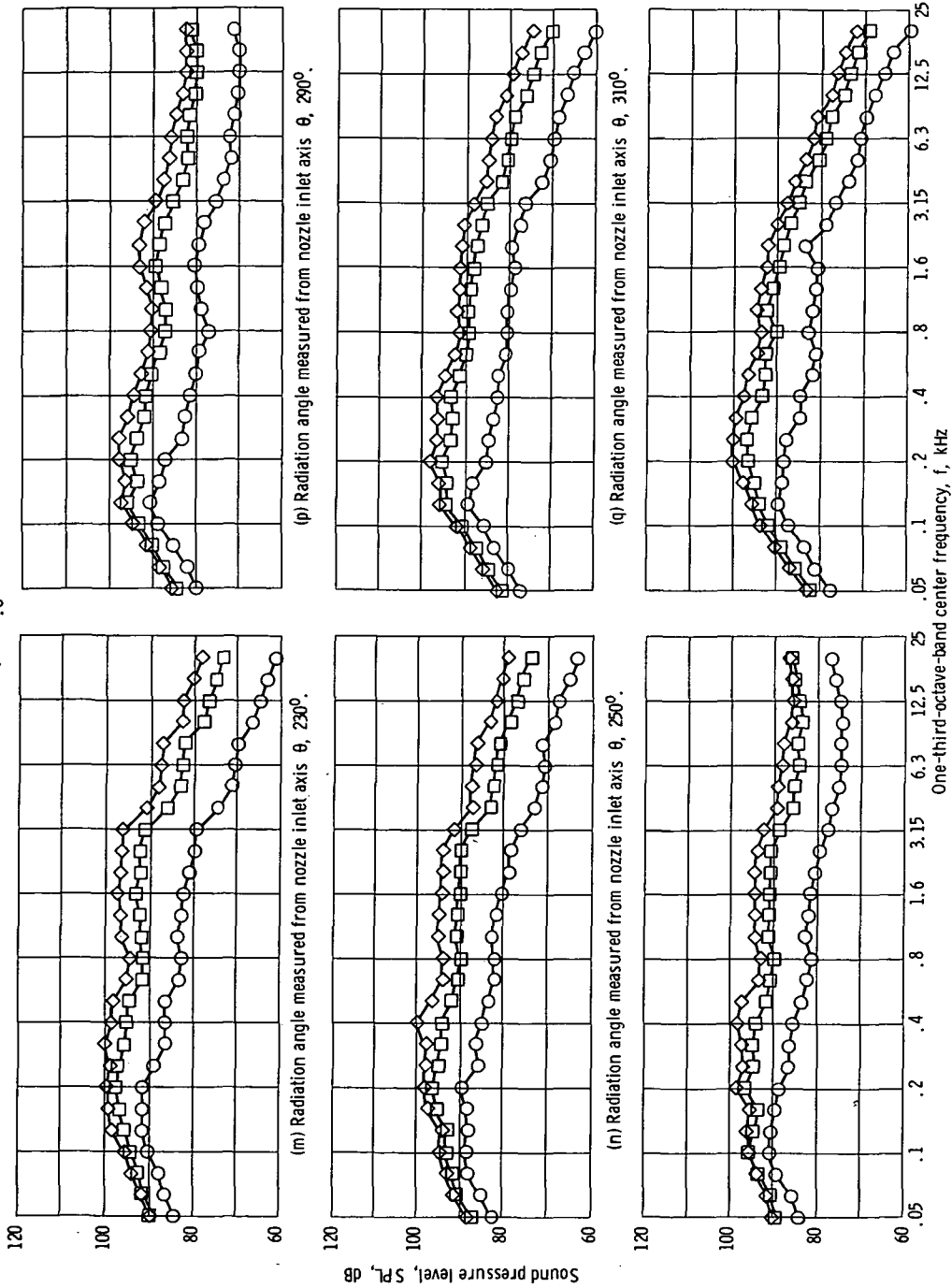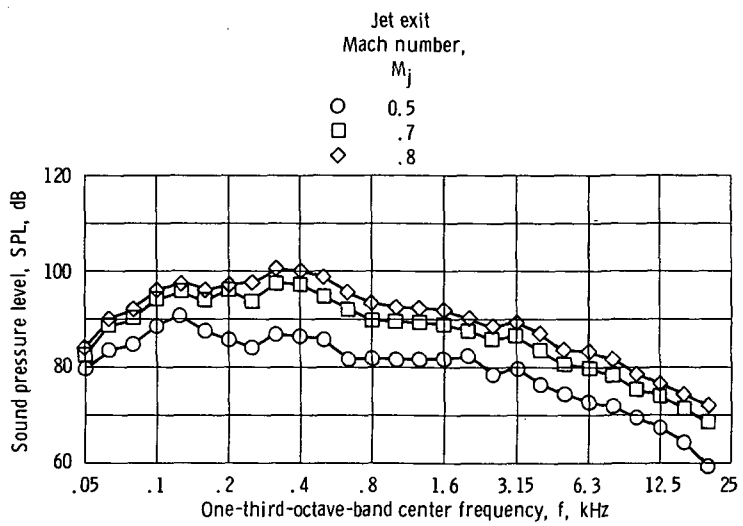(o) Radiation angle measured from nozzle inlet axis θ, 270°.

(p) Radiation angle measured from nozzle inlet axis θ, 290°.

(q) Radiation angle measured from nozzle inlet axis θ, 310°.

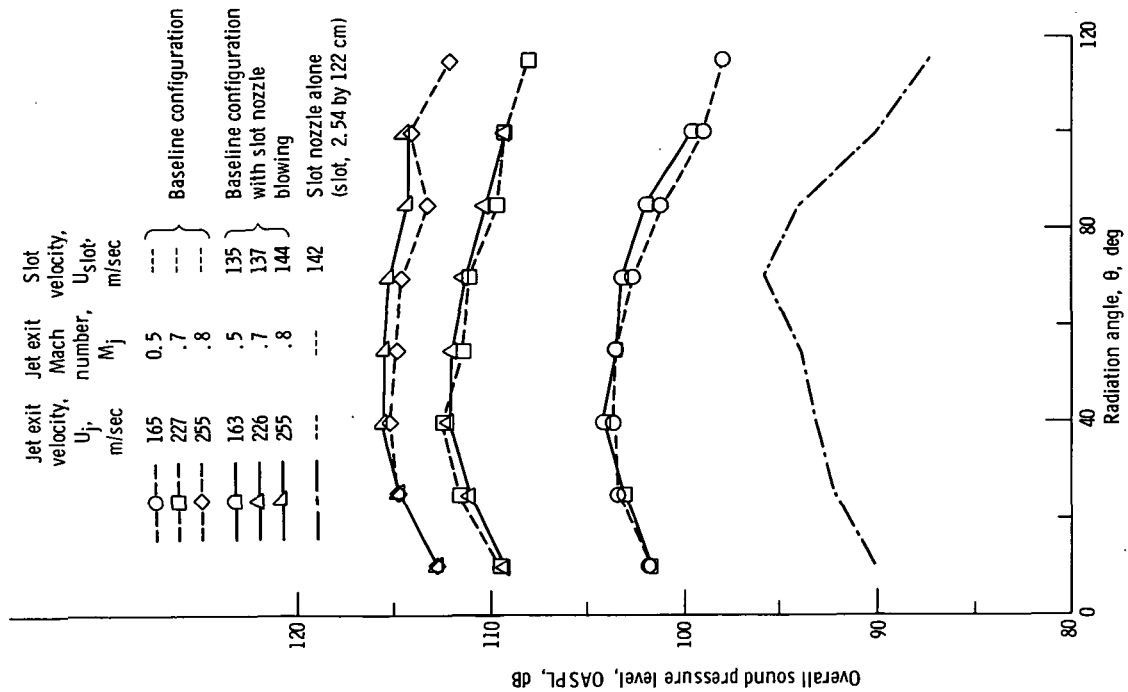(r) Radiation angle measured from nozzle inlet axis θ, 330°.

Figure 14. - Continued.

One-third-octave-band center frequency, f, kHz

Sound pressure level, SPL, dB

Jet exit
Mach number,
$M_j$

○ 0.5
□ .7
◇ .8

46
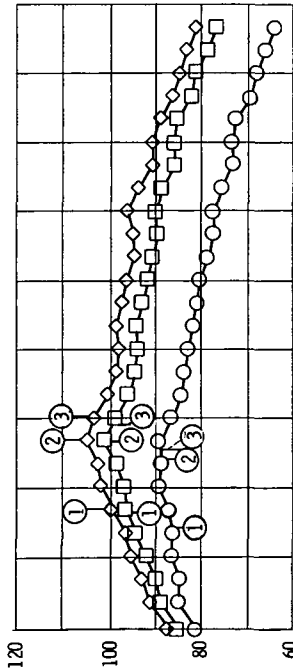
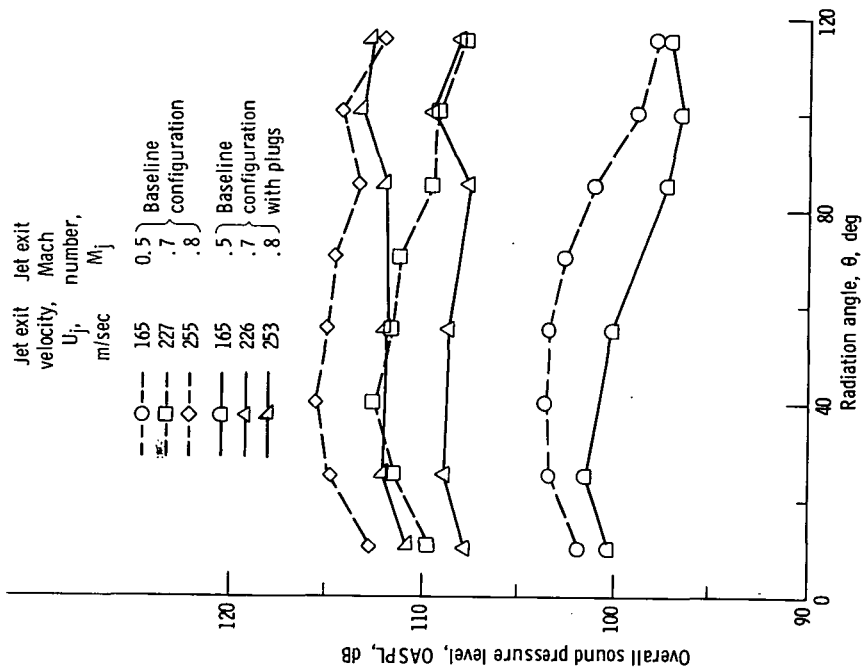(s) Radiation angle measured from nozzle inlet axis θ, 350°.

Figure 14. – Concluded.

Figure 16. - Comparison of overall sound pressure level for baseline configuration and baseline configuration with plugs in slots.

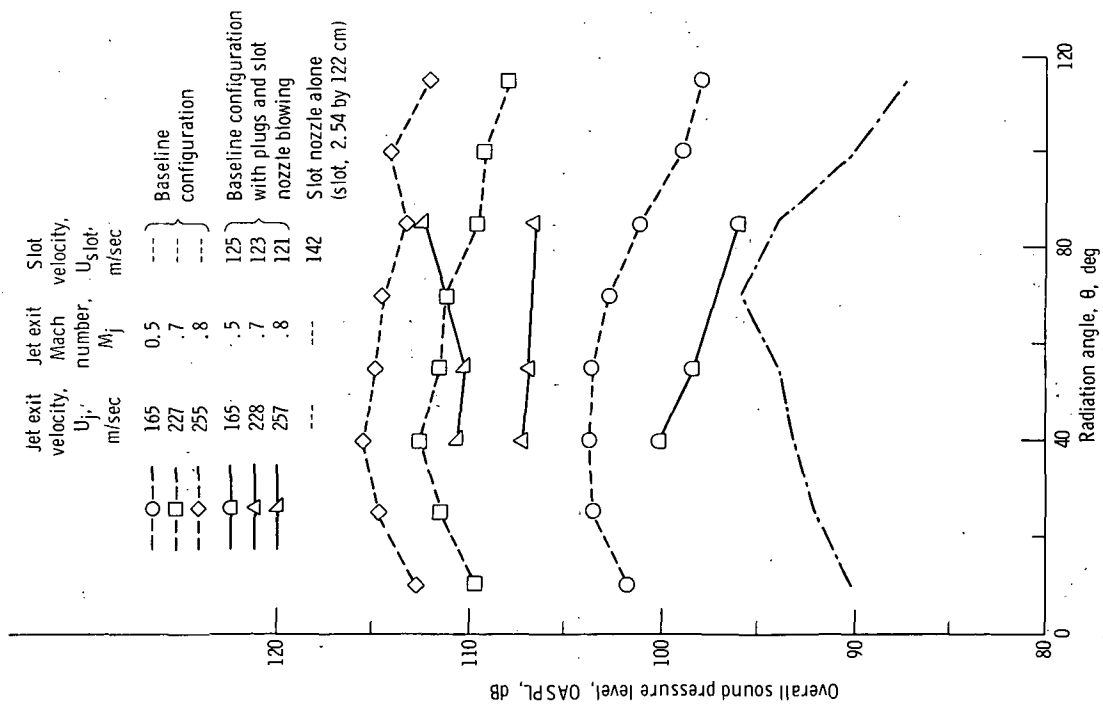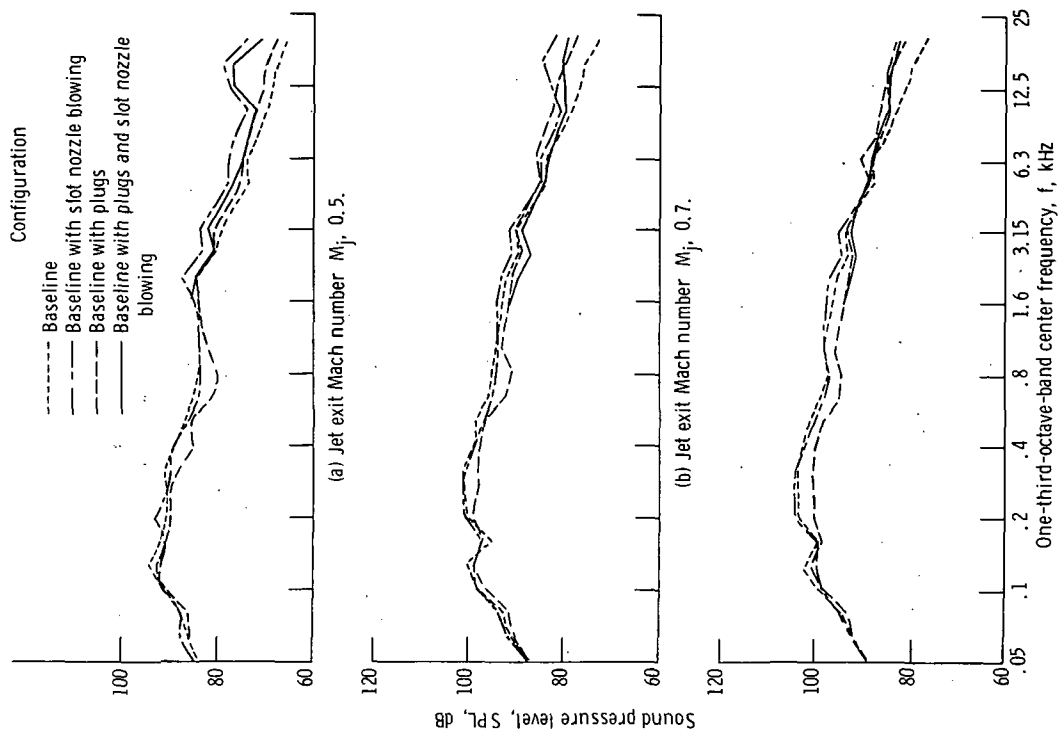| Jet exit velocity, $U_j$, m/sec | Jet exit Mach number, $M_j$ | |
|---|---|---|
| 165 | 0.5 | Baseline configuration |
| 227 | .7 | |
| 255 | .8 | |
| 165 | .5 | Baseline configuration with plugs |
| 226 | .7 | |
| 253 | .8 | |



Figure 15. - Comparison of overall sound pressure level for baseline configuration with and without slot nozzle blowing.

| Jet exit velocity, $U_j$, m/sec | Jet exit Mach number, $M_j$ | Slot velocity, $U_{slot}$, m/sec | |
|---|---|---|---|
| 165 | 0.5 | --- | Baseline configuration |
| 227 | .7 | --- | |
| 255 | .8 | --- | |
| 163 | .5 | 135 | Baseline configuration with slot nozzle blowing |
| 226 | .7 | 137 | |
| 255 | .8 | 144 | |
| --- | --- | 142 | Slot nozzle alone (slot, 2.54 by 122 cm) |

48

Configuration

——— Baseline
——— Baseline with slot nozzle blowing
——— Baseline with plugs
———— Baseline with plugs and slot nozzle blowing

(a) Jet exit Mach number $M_j$, 0.5.

(b) Jet exit Mach number $M_j$, 0.7.

(c) Jet exit Mach number $M_j$, 0.8.

Sound pressure level, SPL, dB

One-third-octave-band center frequency, f, kHz

Figure 18. – Comparison of sound-pressure-level spectra for four configurations at radiation angle of 10°.



| Jet exit velocity, $U_j$, m/sec | Jet exit Mach number, $M_j$ | Slot velocity, $U_{slot}$, m/sec | |
|---|---|---|---|
| 165 | 0.5 | --- | Baseline configuration |
| 227 | .7 | --- | |
| 255 | .8 | --- | |
| 165 | .5 | 125 | Baseline configuration with plugs and slot nozzle blowing |
| 228 | .7 | 123 | |
| 257 | .8 | 121 | |
| --- | --- | 142 | Slot nozzle alone (slot, 2.54 by 122 cm) |

Overall sound pressure level, OASPL, dB

Radiation angle, θ, deg

Figure 17. – Comparison of overall sound pressure level for baseline configuration and baseline configuration with plugs in slots and slot nozzle blowing.

Configuration

- - - - - Baseline
——— Baseline with slot nozzle blowing
— - — Baseline with plugs
————— Baseline with plugs and slot
          nozzle blowing

(a) Jet exit Mach number $M_j$, 0.5.

(b) Jet exit Mach number $M_j$, 0.7.

(c) Jet exit Mach number $M_j$, 0.8.

Sound pressure level, SPL, dB

One-third-octave-band center frequency, f, kHz

Figure 20. - Comparison of sound-pressure-level spectra for four configura-
tions at radiation angle of 40°.

Configuration

- - - - - Baseline
——— Baseline with slot nozzle blowing
— - — Baseline with plugs

(a) Jet exit Mach number $M_j$, 0.5.

(b) Jet exit Mach number $M_j$, 0.7.

(c) Jet exit Mach number $M_j$, 0.8.

Sound pressure level, SPL, dB

One-third-octave-band center frequency, f, kHz

Figure 19. - Comparison of sound-pressure-level spectra for three configu-
rations at radiation angle of 25°.
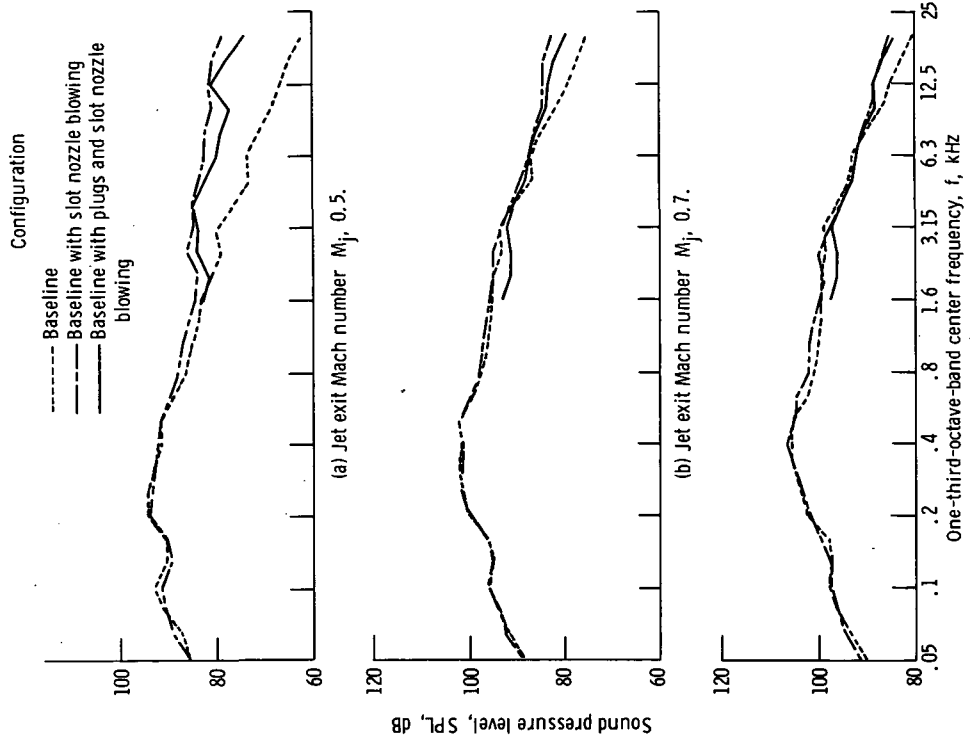
Figure 21. – Comparison of sound-pressure-level spectra for four configurations at radiation angle of 55°.
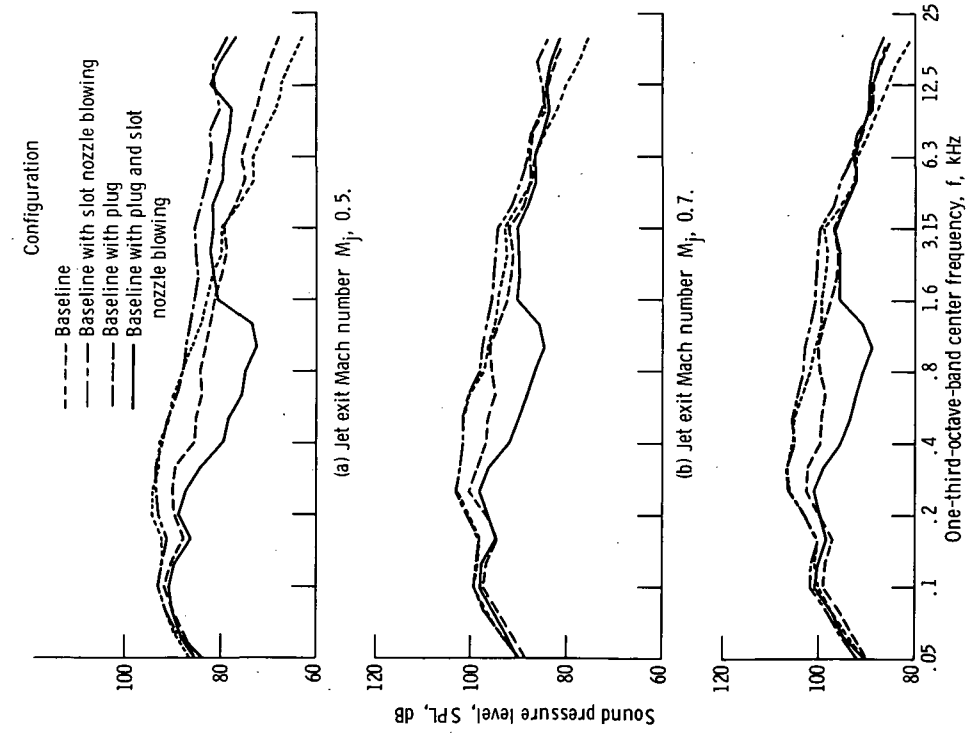
Figure 22. – Comparison of sound-pressure-level spectra for three configurations at radiation angle of 70°.
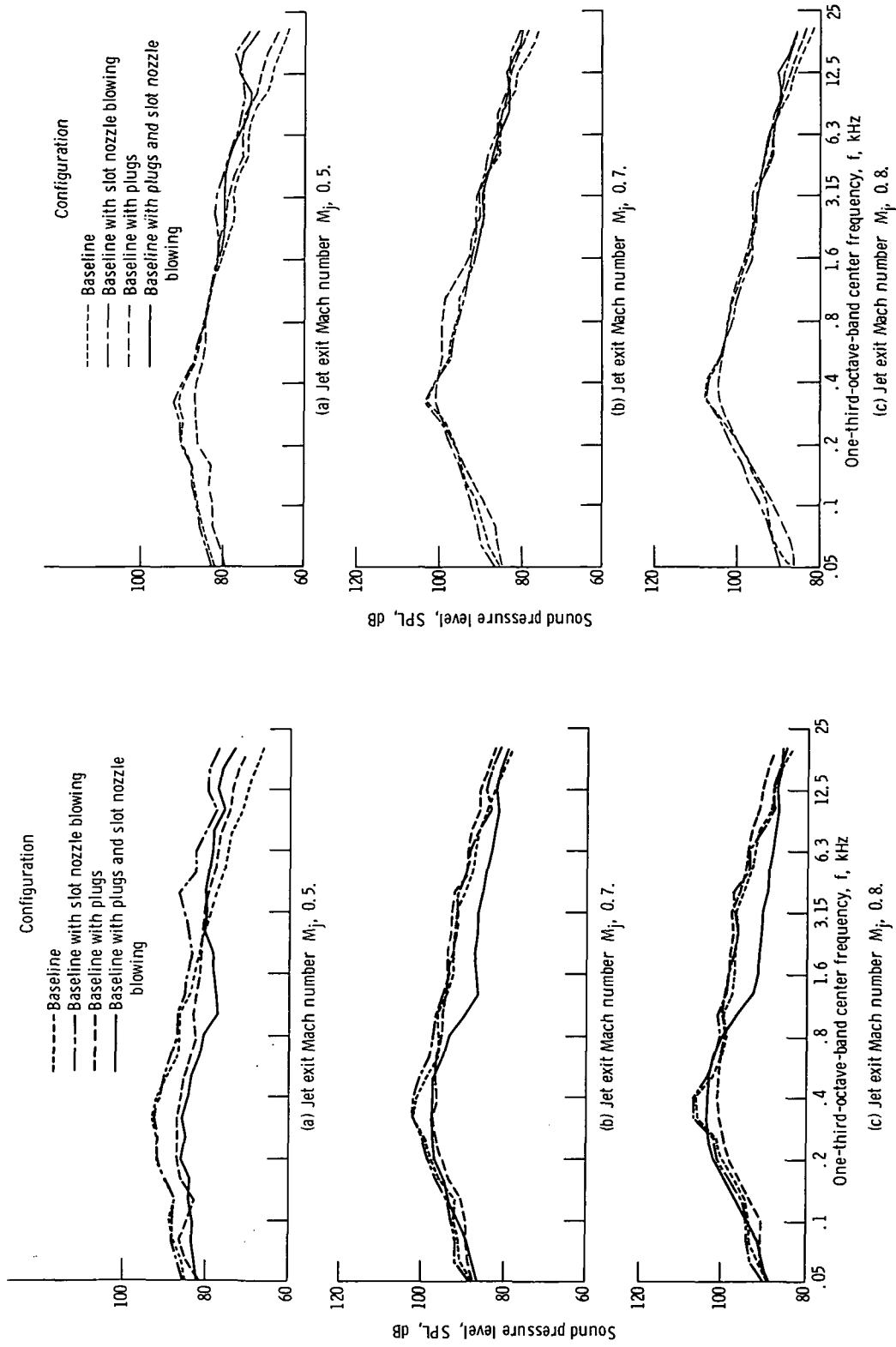
51

Figure 23. - Comparison of sound-pressure-level spectra for four configurations at radiation angle of 85°.



Figure 24. - Comparison of sound-pressure-level spectra for four configurations at radiation angle of 100°.
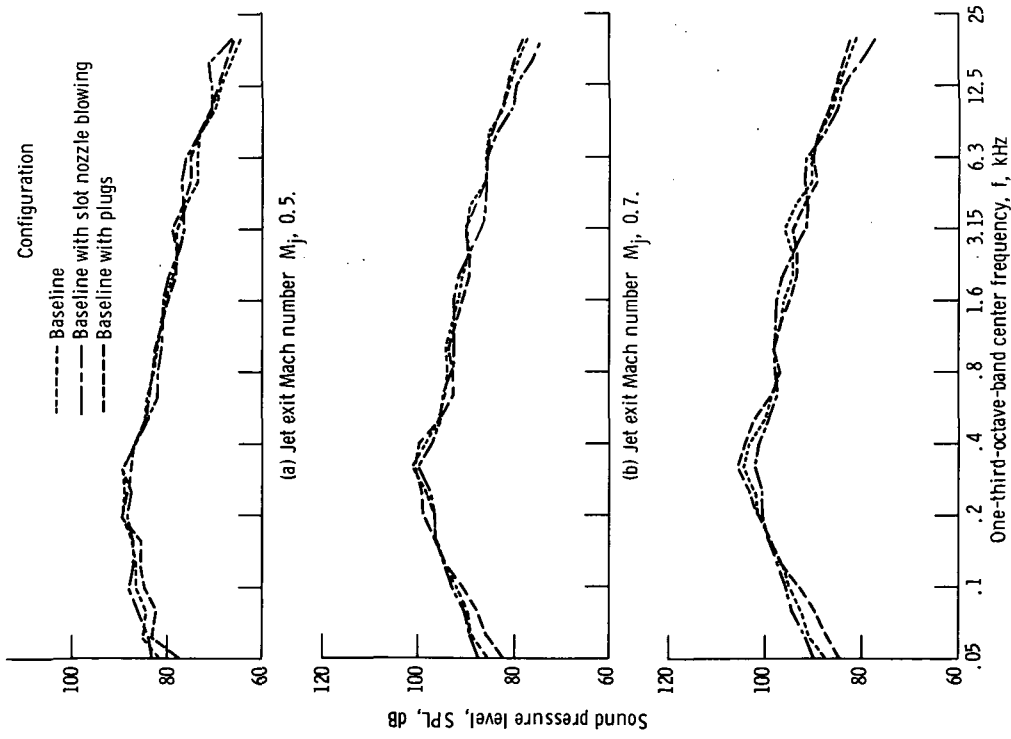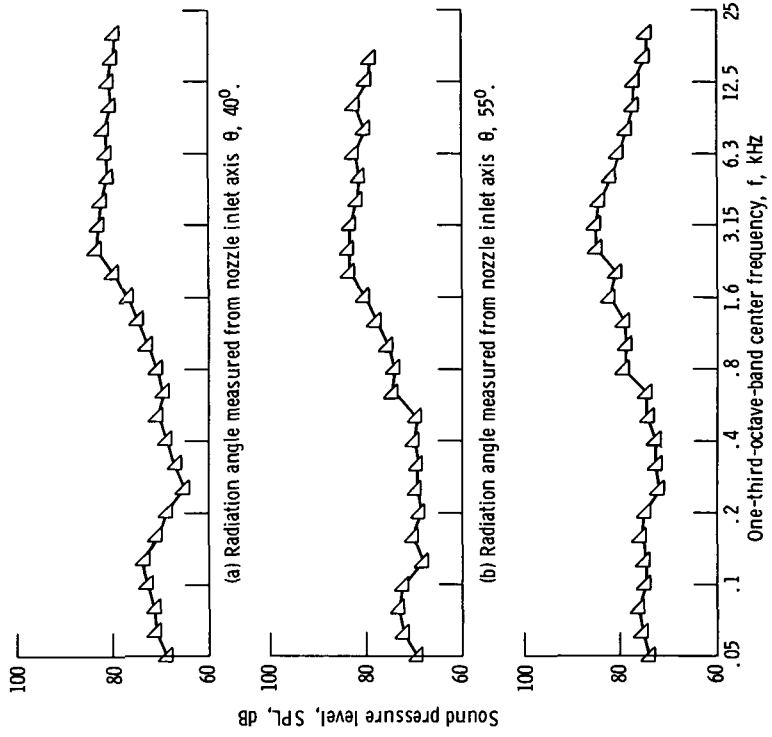
(a) Radiation angle measured from nozzle inlet axis θ, 40°.

(b) Radiation angle measured from nozzle inlet axis θ, 55°.

(c) Radiation angle measured from nozzle inlet axis θ, 85°.

Figure 26. - Sound-pressure-level spectra for slot nozzle only. Slot velocity, 142 meters per second; slot dimensions, 2.54 by 122 centimeters.
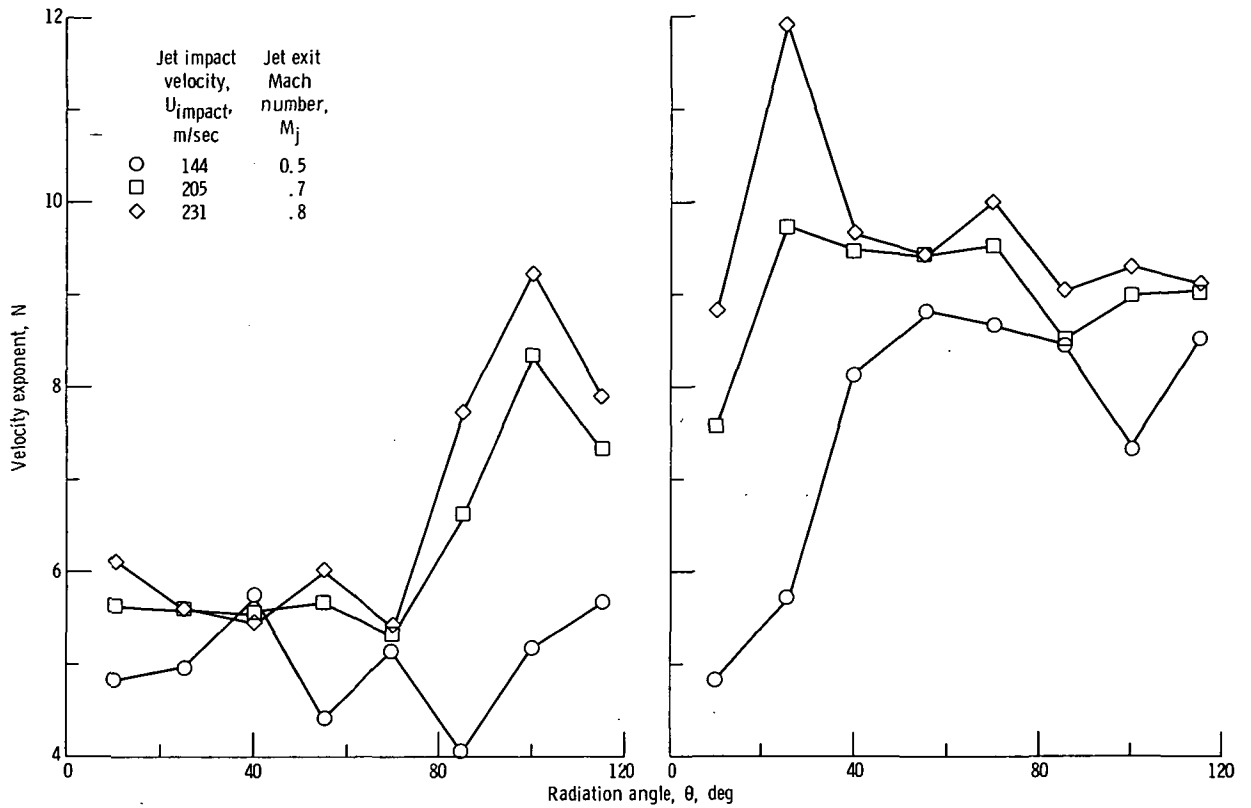


Configuration
—— Baseline
—— Baseline with slot nozzle blowing
—— Baseline with plugs

(a) Jet exit Mach number M_j, 0.5.

(b) Jet exit Mach number M_j, 0.7.

(c) Jet exit Mach number M_j, 0.8.

Figure 25. - Comparison of sound-pressure-level spectra for three configurations at radiation angle of 115°.

(a) Low-frequency range, 50 to 800 hertz.

(b) High-frequency range, 3.15 to 20 kilohertz.

Figure 27. – Distribution of velocity exponent for externally blown flap baseline configuration based on impingement velocity.
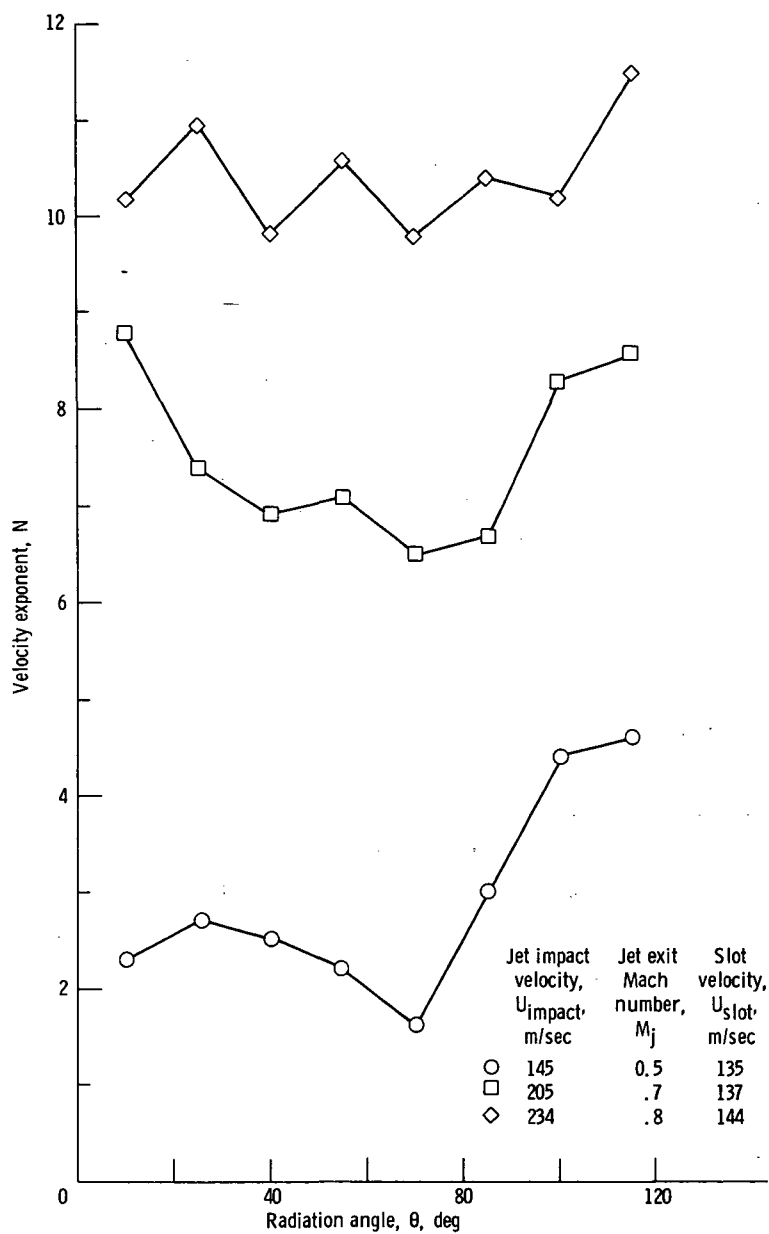
Figure 28. - Distribution of velocity exponent for externally blown flap baseline configuration with slot nozzle blowing. Based on impingement velocity; high-frequency range, 3.15 to 20 kilohertz.
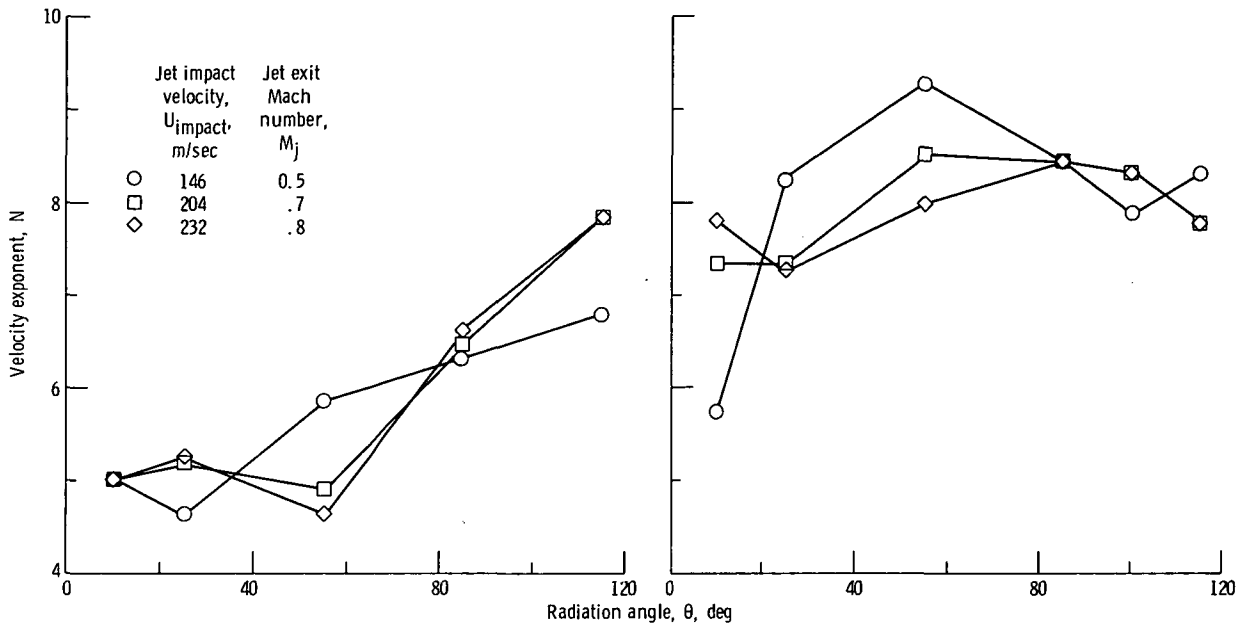
(a) Low-frequency range, 50 to 800 hertz.    (b) High-frequency range, 3.15 to 20 kilohertz.

Figure 29. – Distribution of velocity exponent for externally blown flap baseline configuration with plugs. Based on impingement velocity.
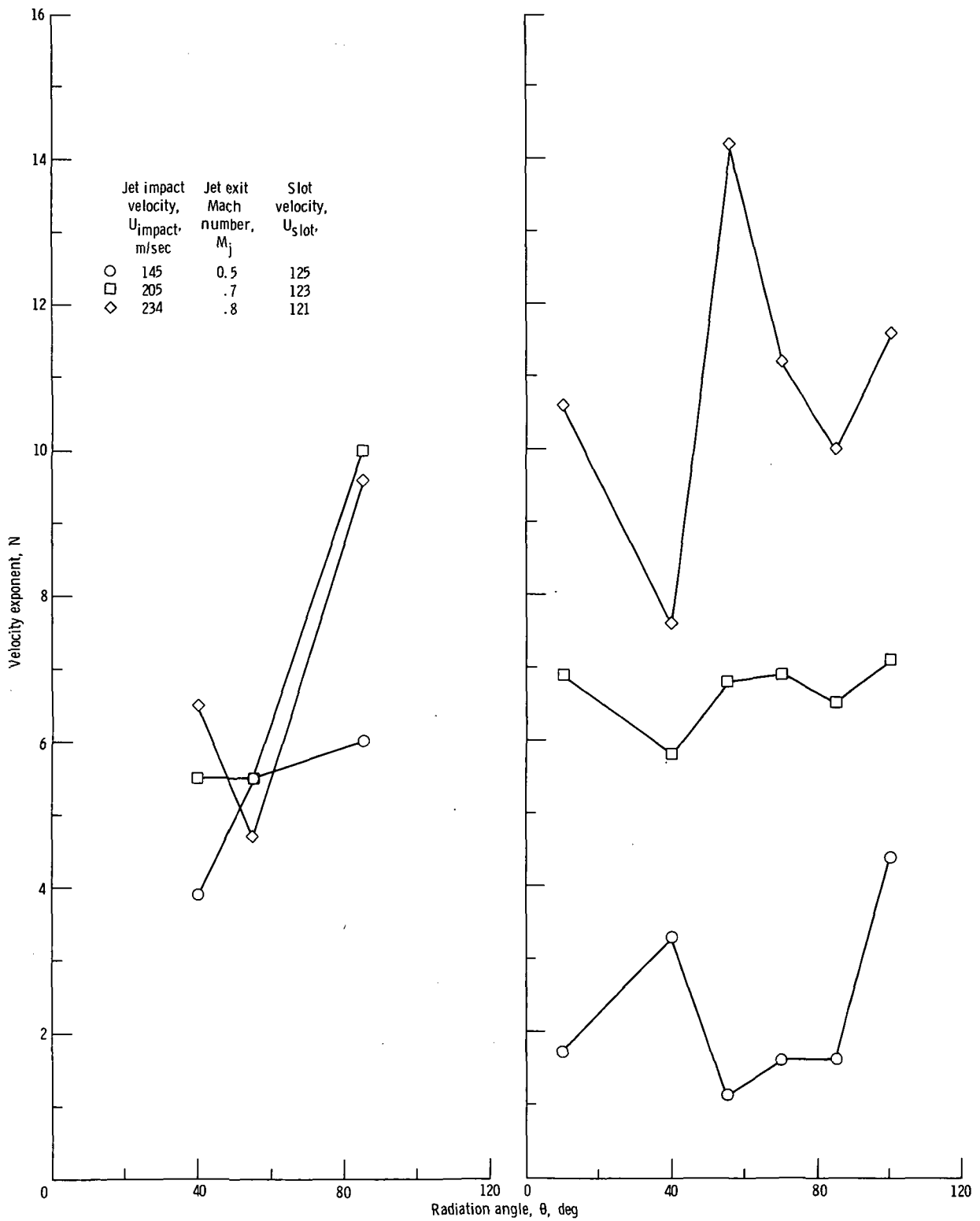
(a) Low-frequency range, 50 to 1000 hertz.

(b) High-frequency range, 4 to 20 kilohertz.

Figure 30. – Distribution of velocity exponent for externally blown flap baseline configuration with plugs and slot nozzle blowing. Based on impingement velocity.
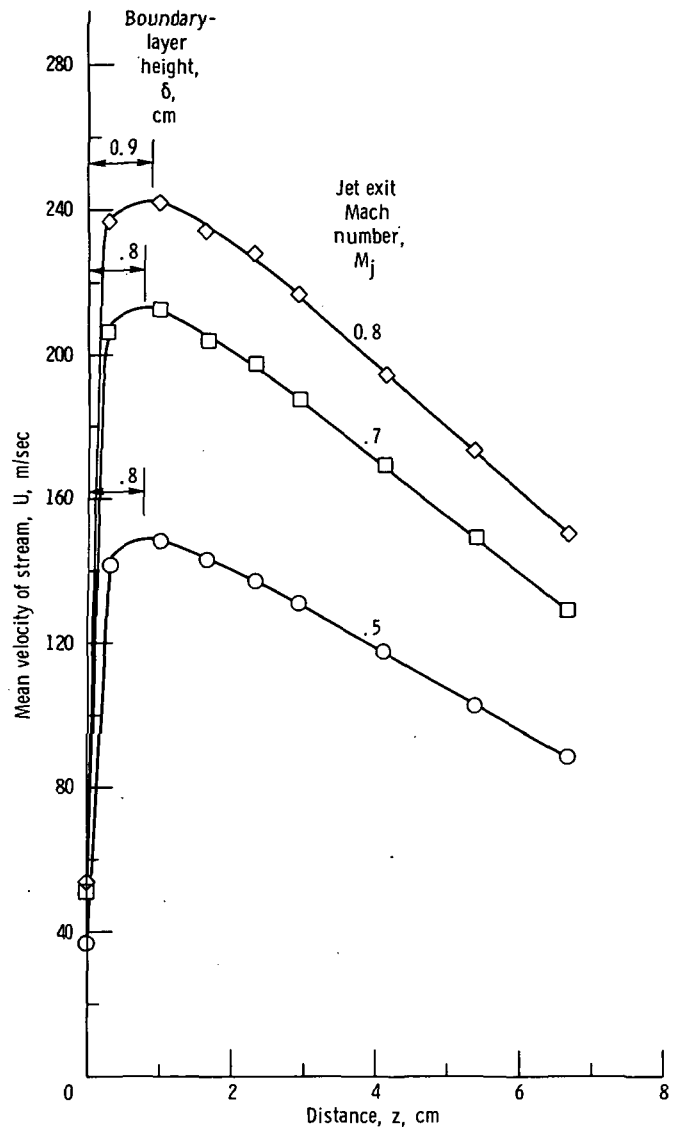
Figure 31. – Velocity profiles in z-direction at trailing edge of second
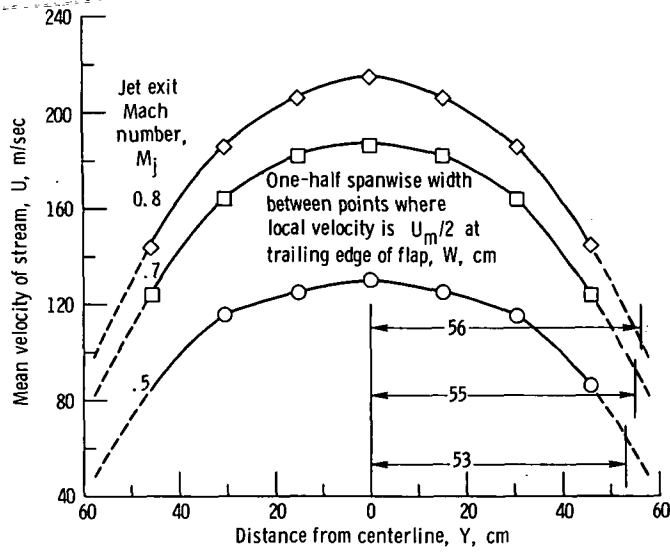flap on jet axis (z'/D = 7. 33) showing boundary-layer height.

Figure 32. - Typical spanwise velocity profiles at trailing edge of
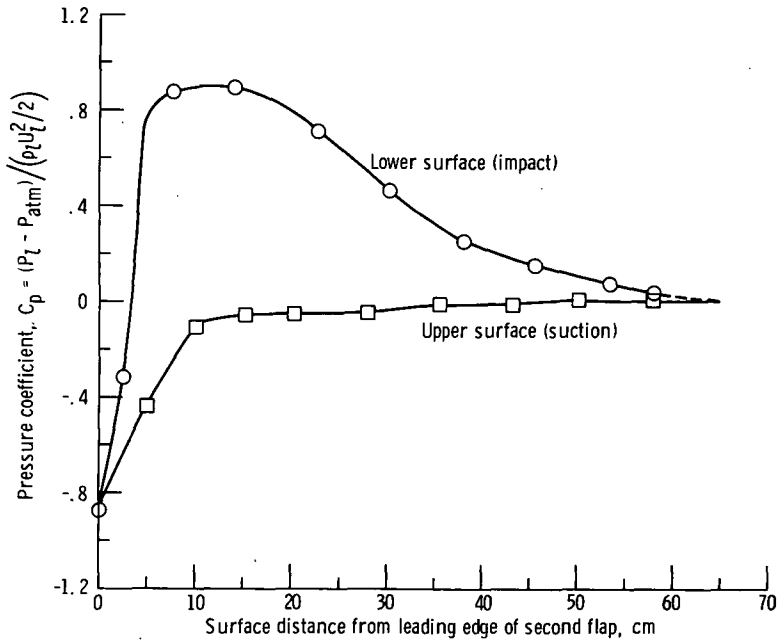second flap 3 centimeters above surface of flap.



Figure 33. - Typical pressure-coefficient distribution around surface of second
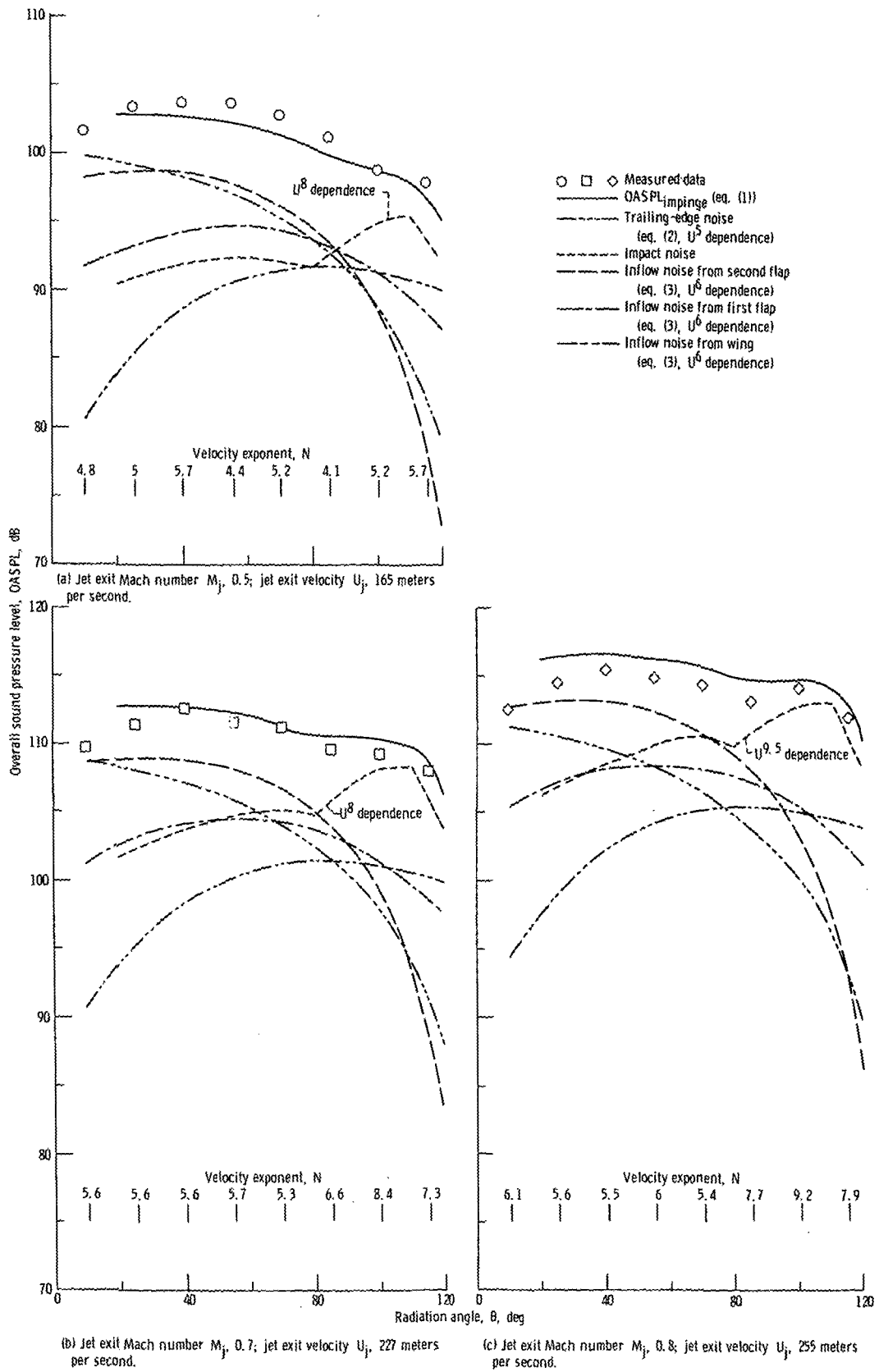flap in plane of jet axis at jet exit Mach number of 0.7.

(a) Jet exit Mach number $M_j$, 0.5; jet exit velocity $U_j$, 165 meters per second.

(b) Jet exit Mach number $M_j$, 0.7; jet exit velocity $U_j$, 227 meters per second.

(c) Jet exit Mach number $M_j$, 0.8; jet exit velocity $U_j$, 255 meters per second.
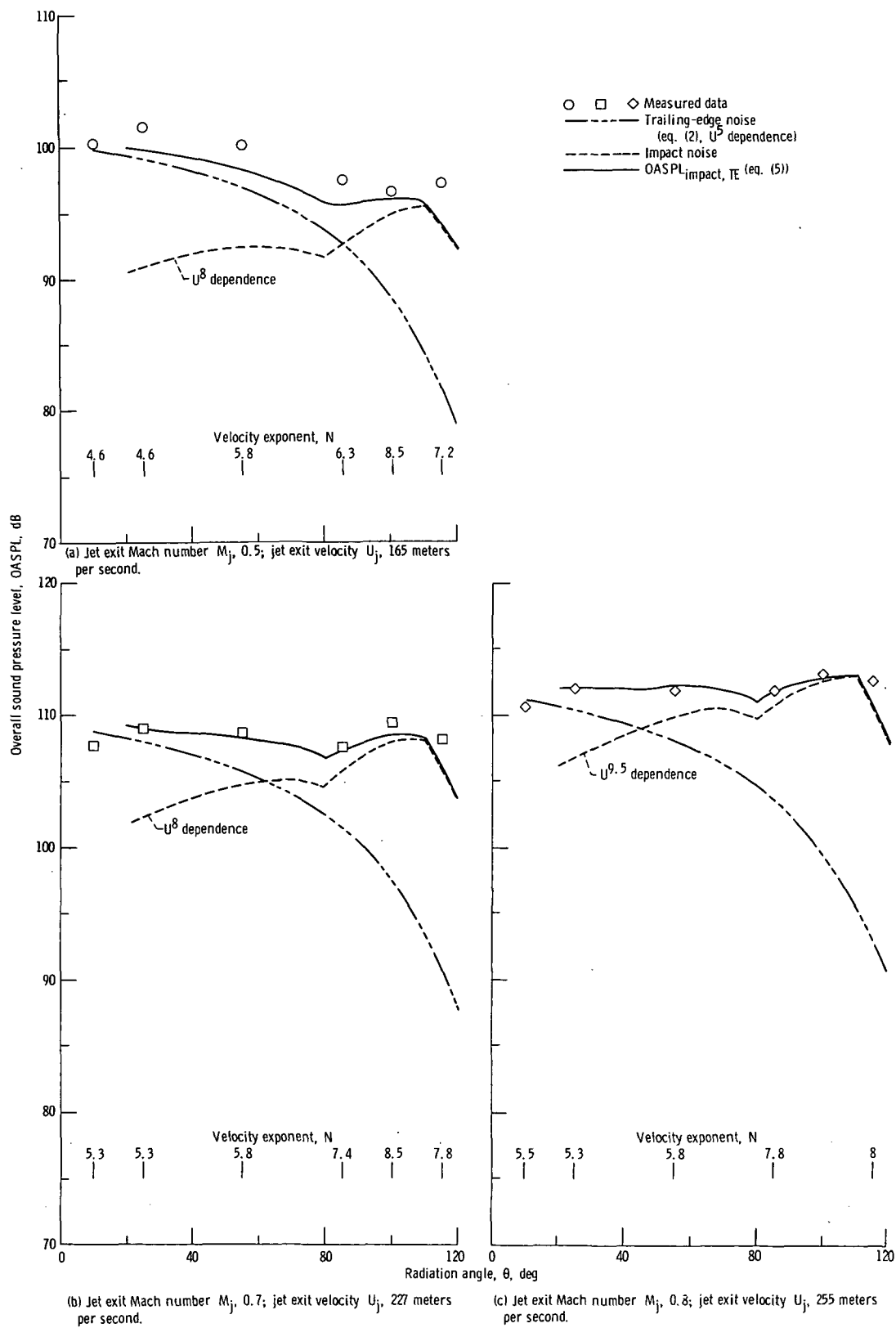
Figure 34. - Comparison of measured and calculated overall sound pressure level for baseline configuration.

Figure 35. – Comparison of measured and calculated overall sound pressure level for baseline configuration with plugs.
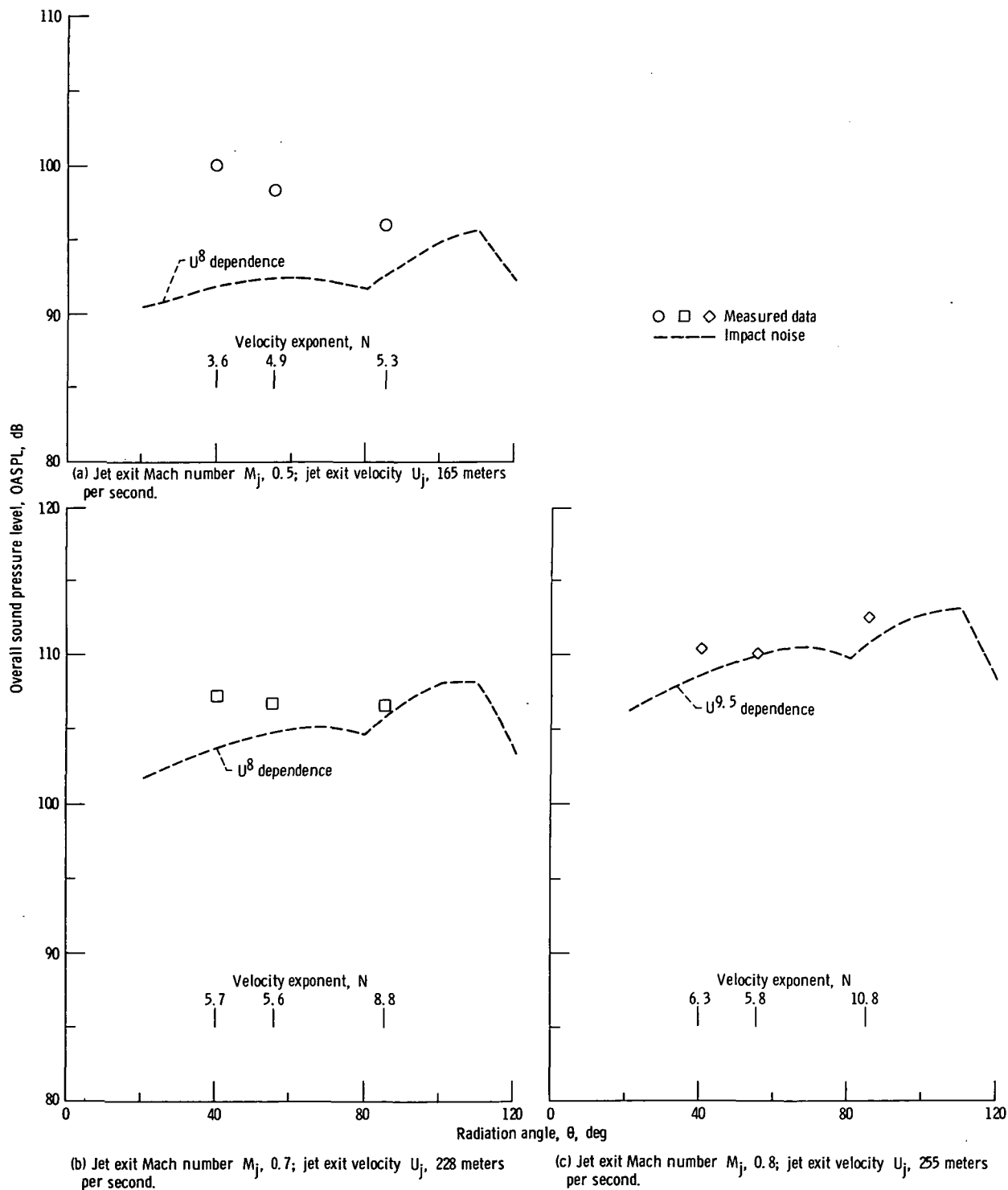
(a) Jet exit Mach number $M_j$, 0.5; jet exit velocity $U_j$, 165 meters per second.

(b) Jet exit Mach number $M_j$, 0.7; jet exit velocity $U_j$, 227 meters per second.

(c) Jet exit Mach number $M_j$, 0.8; jet exit velocity $U_j$, 255 meters per second.

(a) Jet exit Mach number $M_j$, 0.5; jet exit velocity $U_j$, 165 meters per second.

(b) Jet exit Mach number $M_j$, 0.7; jet exit velocity $U_j$, 228 meters per second.

(c) Jet exit Mach number $M_j$, 0.8; jet exit velocity $U_j$, 255 meters per second.

Figure 36. – Comparison of measured and calculated overall sound pressure level for baseline configuration with plugs and slot nozzle blowing.

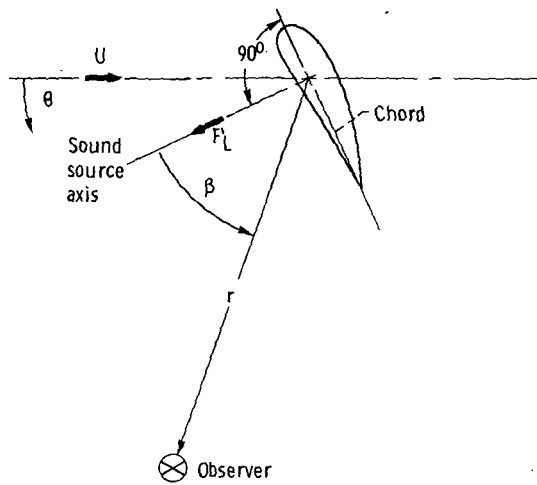Figure 37. – Coordinate system for fluctuating lift force.

*"The aeronautical and space activities of the United States shall be conducted so as to contribute . . . to the expansion of human knowledge of phenomena in the atmosphere and space. The Administration shall provide for the widest practicable and appropriate dissemination of information concerning its activities and the results thereof."*
—NATIONAL AERONAUTICS AND SPACE ACT OF 1958

# NASA SCIENTIFIC AND TECHNICAL PUBLICATIONS

TECHNICAL REPORTS: Scientific and technical information considered important, complete, and a lasting contribution to existing knowledge.

TECHNICAL NOTES: Information less broad in scope but nevertheless of importance as a contribution to existing knowledge.

TECHNICAL MEMORANDUMS: Information receiving limited distribution because of preliminary data, security classification, or other reasons. Also includes conference proceedings with either limited or unlimited distribution.

CONTRACTOR REPORTS: Scientific and technical information generated under a NASA contract or grant and considered an important contribution to existing knowledge.

TECHNICAL TRANSLATIONS: Information published in a foreign language considered to merit NASA distribution in English.

SPECIAL PUBLICATIONS: Information derived from or of value to NASA activities. Publications include final reports of major projects, monographs, data compilations, handbooks, sourcebooks, and special bibliographies.

TECHNOLOGY UTILIZATION PUBLICATIONS: Information on technology used by NASA that may be of particular interest in commercial and other non-aerospace applications. Publications include Tech Briefs, Technology Utilization Reports and Technology Surveys.

*Details on the availability of these publications may be obtained from:*

## SCIENTIFIC AND TECHNICAL INFORMATION OFFICE

# NATIONAL AERONAUTICS AND SPACE ADMINISTRATION
Washington, D.C. 20546